

Position as Probability: Self-Supervised Transformers that Think Past Their Training for Length Extrapolation

Philip Lee
 Xenon Labs LLC
 phil@symphonypro.net, phil.hj.lee@gmail.com

May 15, 2025

Abstract

Deep sequence models typically degrade in accuracy when test sequences significantly exceed their training lengths, yet many critical tasks—such as algorithmic reasoning, multi-step arithmetic, and compositional generalization—require robust length extrapolation. We introduce **PRISM**, a **P**robabilistic **R**elative-position **I**mplicit **S**uperposition **M**odel, a novel positional encoding mechanism that enables Transformers to extrapolate accurately up to $10\times$ beyond their training length. PRISM learns continuous relative positions through a differentiable histogram-filter update, preserving position uncertainty via a probabilistic superposition rather than conventional deterministic embeddings. Empirically, PRISM achieves state-of-the-art length extrapolation, successfully generalizing to previously intractable sequence lengths across algorithmic benchmarks—including arithmetic (addition, multiplication), SCAN compositionality tasks, and complex copy variants derived from DeepMind’s recent datasets. Our analysis demonstrates that PRISM’s stochastic positional encoding maintains sharp and interpretable internal states, providing a theoretical basis for reliable length generalization. These results advance the goal of neural sequence models that remain algorithmically robust at lengths far exceeding their training horizon.

1 Introduction

Motivation & Contribution

Deep sequence models excel when test-time sequence lengths closely match those encountered during training. However, performance sharply deteriorates once sequences grow substantially longer. Despite this limitation, numerous practical applications—from multi-step arithmetic and compositional reasoning to program synthesis and dialogue modeling—require reasoning across sequence lengths that vastly exceed what models typically encounter during training.

Thus, a fundamental open challenge is:

*How can we equip neural sequence models with **length extrapolation** capabilities—the ability to reliably apply learned reasoning algorithms to sequences far longer than those observed during training?*

In this paper, we present **PRISM**¹, a probabilistic relative-position encoding scheme based on a *non-stationary, learnable histogram filter*. Inserted into a Transformer, PRISM substantially

¹Code and pretrained models will be released soon.

extends length generalization capabilities, achieving accurate extrapolation by hundreds of timesteps on various challenging algorithmic benchmarks. Our approach significantly outperforms standard Transformer positional encodings, enabling:

- **Arithmetic generalization:** Successfully extrapolating chain-of-thought addition and multiplication tasks from training on 10-digit sequences to over 30-digit sequences, without using explicit index hints.
- **Compositional reasoning:** Achieving near-perfect accuracy on extended variants of the SCAN dataset, even at the maximum test sequence length.
- **Advanced copy tasks:** Reliably handling complex duplication, reversal, and dynamic string-copy tasks at sequence lengths up to $15\times$ beyond training horizons.
- **Algorithmic reasoning tasks (Ruoss et al., 2023):** Robustly generalizing on "odds-first," "bucket sort," and stack manipulation tasks derived from recent DeepMind benchmarks.

Crucially, PRISM maintains a categorical distribution over positional embeddings, effectively preserving uncertainty through a probabilistic superposition rather than collapsing to deterministic averages. This design ensures sharp, interpretable attention and robust generalization even at unprecedented sequence lengths.

Length extrapolation is essential for robust generalization: without it, language models fail to reliably extend learned reasoning patterns beyond limited synthetic curricula². By introducing PRISM, we establish a foundation for neural architectures that consistently execute algorithmic reasoning at previously inaccessible sequence scales, paving the way for reliable real-world applications.

Interpretability and analysis. Because the histogram filter is a small, closed-form subroutine, we can derive an exact *non-stationary Hidden Markov Model* that underlies the architecture. This connection yields:

- A rigorous explanation for **why** extrapolation succeeds, formalized in new theorems,
- an efficient $\mathcal{O}(P)$ update rule (Alg. 1) that avoids the $\mathcal{O}(P^2)$ cost of a naïve dense transition, and
- diagnostic visualizations of the position histogram that make the model’s internal “program counter” human-readable.

Taken together, these contributions advance the goal of building *language models that remain reliable on task execution even when the problem length far exceeds the training horizon*. Furthermore, our results reflect, to the best of our knowledge, the first neural network architecture that demonstrates extrapolation on a variety of simple algorithmic reasoning tasks **via a purely self-supervised approach**. Thus, we believe that our work sheds new light on a **possible path towards human-level extrapolation on practical long-horizon tasks that require chains of thought as well as other forms reasoning that may be derived from self-supervision**.

²As a thought experiment, understanding a long program that was never observed in the training data, such as idiosyncratic spaghetti code, would require tracing the program in terms of its most basic instructions, instead of using heuristics; an LLM reasoning system that only understands programs up to the training horizon may fail to understand the simplest of programs.

2 Overview

We formalize a differentiable update rule for tracking distributions over discrete positions, used for modeling relative positional encoding in a neural architecture for solving arithmetic and other algorithmic reasoning tasks. The update can be seen as the propagation of a probability distribution (histogram) via a learned stochastic matrix at each time step, akin to a nonstationary hidden Markov model. At every position in the sequence, the model maintains a *categorical distribution* (not just a mean) over positions, enabling a *superposition* of positional embeddings and achieving length generalization.

3 Related Work: Length Extrapolation in Transformers and other Sequence Models

3.1 Recent Position–Extrapolation Landscape

Recent work has revived classical algorithmic evaluations—*copy*, *reverse*, *addition*, *sort*, *SCAN*—as litmus-tests for a transformer’s ability to *generalize beyond the training length*. Table 1 summarizes the principal approaches; we highlight below how they differ from our **learned stochastic distance** formulation.

Positional *ablation* and randomization. Kazemnejad et al. [13] show that simply *removing* positional encodings (NOPE) already beats many static schemes on copy/SCAN, though extrapolation remains very limited on all tasks measured. Ruoss et al. [22] push this idea by feeding *fresh i.i.d. Gaussian* encodings each step; the model learns to ignore them, but extrapolation is measured only in *token-wise* accuracy on binary outputs ($\approx 50\%$ random baseline). **Our model** instead *learns* a probabilistic distance without discarding positional information, achieving exact-match figures on arithmetic that these random-or-absent baselines cannot approach.

Explicit *index hints* and similar hard-coded features. Abacus Embeddings [17], Position Coupling ([cho2024coupling]), and the systematic study by Zhou et al. [31] encode *hard-wired landmarks* (e.g. per-digit starts or left/right couplets) that tell the network *exactly* which tokens must align. This yields impressive accuracy (e.g. 99% on 100-digit addition) but at the cost of hand-crafted supervision; performance collapses once the landmark pattern changes. In contrast, our reset/increment/decrement gates discover *their own* landmarks, with no task-specific annotations.

Hard-ALiBi (Jelassi et al., 2024) and other hashing-based retrieval approaches. Hard-ALiBi fixes one attention head with a global *ALiBi* bias and constrains all remaining heads to a local n -token window. During the *copy* task, each local head hashes its current length- n block, while the global head retrieves the token that followed the *same* hash earlier in the sequence. Trained on 50-token inputs, the model attains over 95% string-level accuracy on 1000-token copies. However, because the hash is computed over a fixed n -gram, the method breaks when an n -gram appears twice (hash collisions), preventing reliable copying of sequences with repeated substrings—e.g. character-level inputs such as ‘aaaa...’, or the repeated *character-level tokens* in our arithmetic, algorithmic reasoning, and general copy benchmarks.

In other words, our approach imposes *no* uniqueness constraint³ and still achieves exact-match accuracy, highlighting the benefit of a fully learned relative distance metric instead of generating such lookup tables. In all of our training and test setups, we *require* that models be able to perform both character and non-character level manipulations, regardless of whether any vocab tokens are used multiple times in the context. Thus, we assume the conditions of any realistic self-supervised learning setting.

Furthermore, we construct no structure (e.g. hash tables, previous token pointers) that is built around performance on a specific task, including the copying of tokens from left-to-right order, as in Jelassi et al. 2024. In several of our visualizations, we further highlight the importance of copying from a previous position that is not even mapped 1:1 with any of the later token positions. For example, when performing CoT addition (figure 16), our cursor must advance to the next position after every 5 tokens - the length of each CoT step - in order to retrieve the next pair of digits being added for the next CoT step. This is in contrast to exact string duplication used here, which, by construction, must match the output n -gram 1:1 with the *same* earlier n -gram, provided that *all matching pairs of n -grams are unique pairs*. The latter is precisely the condition imposed by Jelassi et al. 2024, and thus, it offloads much work to an external program: a "unique" n -gram can in principle be set equal (at runtime) to the entire input sequence to be copied, making the task trivial for the LM while collapsing all of the context to a single token.

For such work imposing unique token constraints, including Jelassi et al. 2024, Barbero et al. 2024, and [2024], *learned* relative position encodings are lacking, as they are complementary approaches. Similar to *index hints*, hashing-based approaches hard-wire the pairs of tokens that are aligned: their long-range retrieval abilities depend on attending to the hashed string. Unique/hashed tokens also impose no structure that satisfies the conditions of a *distance function* that is the focus of this work.

Fixed or data-adaptive biases. Duan et al. [4] calibrate *static (hard-coded, unlearned)* attention biases to mimic certain attention patterns that boost extrapolation; extrapolation is thus predetermined. Zheng et al. [30] learn a *token-wise bias* for up to 40 digit binary addition, and no index hints, and report 60.8% *per-token* accuracy at lengths 41 – 400, which is much less than the accuracy required for extrapolation. In contrast, we use chain of thought, and only use *exact match accuracy* as our metric. Our histogram update is data-adaptive and operates on an explicit, *learnable distribution* over positions; empirical results (§7) show sharp exact-match retention on algorithmic extrapolation.

Recurrent or looped computation. The *Looped Transformer* [8] obtains perfect accuracy on binary addition without chain of thought. Intriguingly, accurate output is generated only when looped *exactly* the ground-truth number of recurrent steps, which the authors have predetermined based on the RASP [28] runtime complexity of each problem instance; accuracy drops to zero if run shorter or longer.

Analysis of the model from the authors has shown that the sensitivity to the number of recurrences is due to the model *shifting* its input tokens to the correct output positions, with the number of shifts proportional to the input length. Shifting in proportion to sequence length limits the efficiency and flexibility of their approach. The Looped Transformer also uses no position encoding,

³Nor do we use multi-character tokenization for arithmetic and copying-like tasks

nor chain-of-thought tokens.

The fixed number of recurrent steps is a predetermined hyperparameter, and part of the supervision signal that the model received during training in order to correlate inputs with the correct outputs. Thus, it is a counter that must also be supplied at test time.

Delétang et al. [3] demonstrate that an RNN controller (*Tape RNN*) with structured memory, and provided a read/write head that can jump left or right a number of positions l before writing to the tape, where l is the *input sequence length* provided at train and test time to the model, can generalize well on tasks like binary addition, reversing binary strings, and recognizing & generating context-sensitive grammars on other binary inputs. In contrast, we do not provide any external supervision signal, including signals dependent on the length of the input (resp. *Tape RNN*) or predetermined problem complexity (resp. *Looped Transformer*). Furthermore, our architecture is designed to work with both RNN and non-RNN based architectures: we only require transformer-like self-attention [26] mechanisms for computing the similarity between arbitrary positions. We also do not provide additional "thinking tokens" for tasks that overlap with [3], specifically Stack Manipulation and Odds First: we instead keep these tasks identical to [22] instead of padding the sequence length or extending these tasks with CoT or "thinking" tokens.

In summary, we take a very different approach to models that require recurrent processing steps, as we do not, for example, write to a structured memory analogous to a *memory tape* that can be overwritten. Second, our training is entirely in the self-supervised regime, and therefore, there is no supervision signal that parametrizes the length or complexity of the input.

Instead, we use transformer self-attention to *autoregressively* (using causal masking) sample tokens, requiring *all* chain of thought tokens (where applicable) to be predicted correctly, and with a single forward pass—no external counter or step supervision. In contrast, Looped Transformer does not use a masked language modeling objective, and all fixed output positions have to be predicted simultaneously at the end of the supervised number of recurrent steps. Finally, core to our approach is learning a **relative positional encoding** (relative distance function) between arbitrary tokens.

Language-modeling extrapolation. BiPE [11], CABLE [1], and other works we have comprehensively surveyed target document-level LM and report lower perplexity at 8–16× the training context. They neither evaluate algorithmic tasks nor require exact match. Our focus is the opposite extreme: *symbolic reasoning* where a single digit error ruins the answer; nevertheless, the same stochastic histogram layer can replace their PE modules and inherits theoretical guarantees discussed in Section 5.1.1.

Hand-labeled positional training data, self-training, and other curricula outside of standard self-supervised settings Recent work [15] has shown that data filtering for too short responses can be a hard-coded proxy that can be used for self-training on longer data by filtering out short responses, which was a crucial supervision signal across all tasks they evaluated. However, there are many problems for which the generated answer is (in principle) independent of the input size. Therefore, we also evaluate performance where the length of the task to complete (i.e. the length of the output tokens) is independent of the input size.

Nonetheless, while approaches that use self-training may improve upon index hints and other train-

ing schemes that require all (relative) positional embedding features to be learned, such as via randomization, context stuffing, or randomly "shifting" the positional encodings for training samples, if the amount of new data is reduced in practical settings, the architecture introduced in this paper makes no assumptions that additional data on longer tasks is required, thus also saving compute and time to develop a model that demonstrates length extrapolation.

Therefore, this work is complementary to self-refinement based approaches for the following reasons: (a) their approaches explicitly keep the vanilla transformer architecture intact, and thereby needs curated or self-curated data on which to train on longer tasks; (b) in contrast, we train a new relative position encoding; (c) we do not require additional data than the initial training data, instead allowing our relative position encoding to capture dependencies that are intrinsic to various tasks in a length-generalizable way; (d) our architecture does not intrinsically require hard-coded or majority voting-dependent data filtering rules on data that is self-generated or otherwise.

Another recent work [9] explored training a standard transformer architecture to predict the coupled position labels of [2]. This follows the basic approach of [2], except that instead of giving the correct position IDs as inputs to the model at *test time*, the correct *position IDs* are part of *ground truth training data* for the model to predict as an objective. Thus, in the training data, two different types of labels are provided for the autoregressive prediction task: the correct next token, and the correct next *coupled position ID* using a separate output projection. While useful in theoretical insights and guarantees, in contrast to their work, (a) our approach relies only on self-supervised learning from the data (i.e. trains *only on text tokens*), and therefore, (b) we do not provide external signals such as *position IDs* as part of the training objective, as no special tokens, nor self-distillation signals, are provided during training or inference. Furthermore, we introduce a new architecture via (c) learning an implicit relative distance function over the observed tokens from self-supervision.

Broader surveys on length extrapolation. While the works discussed above concentrate on *algorithmic* and structured-reasoning tasks, two recent surveys provide a complementary, large-scale view of length extrapolation in language models, encompassing both algorithmic and non-algorithmic reasoning. *Length Extrapolation of Transformers: A Survey from the Perspective of Positional Encoding* [29] catalogues positional-encoding designs up to 2023, covering both fixed and learned schemes (e.g. ALiBi, RoPE, Rotary) as well as early sequence-compression methods. More recently, *Thus Spake Long-Context Large Language Model* [16] focuses on scaling challenges in large-context LLMs (16k–100k tokens), highlighting memory-efficient attention variants, retrieval-augmented models, and curriculum strategies for pre-training. Both surveys emphasize that **learned relative encodings capable of generalizing beyond the training horizon remain an open problem**, especially on tasks that demand exact algorithmic correctness—precisely the area addressed in this work by our PRISM relative position architecture.

Summary. Existing methods either: (i) discard position signals entirely, falling short of accurate extrapolation, (ii) bake in task-specific landmarks, (iii) rely on static distance biases, or (iv) hard-wire the computation length. Our work differs by training entirely from *self-supervised data* (no other supervision signal, hard-coded or otherwise), *learning a full categorical distribution over relative positions* via a sparse stochastic matrix, and by its emphasis on chain-of-thought instead of heuristic, single-step reasoning. Our requirement of predicting all intermediate steps correctly increases the output sequence length that our models must predict by several times (e.g. over 4x on CoT addition). We require training each model from scratch for each task, using a self-supervised

autoregressive training objective. Our work demonstrates that the resulting superposition encoding preserves discriminative sinusoidal phase information essential for long-horizon exact-match reasoning.

Citation (Year)	Task Type	Index Hints?	Learned Distance?	Metric	Key Extrapolation Result
Ruoss et al., “Randomized Positional Encodings” (ACL ’23)	copy, reverse, stack manipulation, boolean	No (randomized)	Learnable and unlearnable RPE	token-accuracy	~ 50 – 80% per-token on binary outputs; +12% avg. accuracy on 15 algorithmic tasks.
Kazemnejad et al., “Impact of Positional Encoding” (NeurIPS ’23)	copy, reverse, SCAN-like	No	No (NoPE)	exact-match	NoPE (no PE) outperforms APE/ALiBi/Rotary on longer inputs. Extrapolation remains very limited across all tasks and models.
Zhou et al., “What Algorithms Can Transformers Learn? A Study in Length Generalization” (ICLR ’24)	copy, reverse, sort	Yes (explicit hints)	No	exact-match	~ 100% at 2× length; drops to 0% by 4×.
Jelassi et al., "Repeat After Me: Transformers are Better than State Space Models at Copying Transformers are Better than State Space Models at Copying" (ICML ’24)	copy	Yes (hashed index)	No	exact-match	95% on 1000-token copy after training on 50; fails when n -grams repeat (hash collisions). Relies on hash table with previous token pointers.
Lee et al. "Teaching Arithmetic to Small Transformers" (ICLR ’24)	addition	No	Implicit	exact-match	0% on 8 digits. Trained to full accuracy on 7 digit addition <i>using chain of thought</i> .
Cho et al., “Position Coupling: Leveraging Task Structure for Improved Length Generalization of Transformers”	addition	Yes (coupled indices)	No	exact-match	~ 95% at 5× training length on arithmetic.
Zheng et al., “DAPE: Data-Adaptive Positional Encoding for Length Extrapolation” (NeurIPS ’24)	copy, reverse, SCAN-like	No	Yes (data-adaptive)	token-accuracy	~ 85% per-token at 4× length on algorithmic tasks.
He et al., “Bi-Level Positional Encoding (BiPE)” (ICML ’24)	long-document QA / summarization	No	Yes (inter-/intra-segment)	ROUGE / accuracy	Outperforms RoPE/ALiBi on 8192-token contexts in QA/summarization.

Table 1: Length-extrapolation methods on algorithmic tasks.

Citation (Year)	Task Type	Index Hints?	Learned Distance?	Metric	Key Extrapolation Result
McLeish et al., “Abacus Embeddings” (NeurIPS ’24)	20→100-digit addition, multiplication, sort	Yes (generalized index hints; per digit index)	No	exact-match	97.9% on 100-digit addition after training on 20-digit; 5× extrapolation.
Transformers Can Achieve Length Generalization But Not Robustly (’24)	40→100-digit addition	Yes (per digit index)	Yes (RoPE, FIRE)	exact-match	99% using index hints+FIRE RPE on 100 digit addition while trained on 40. index hints+RoPE and other PE falls to 0%
Duan et al., “Attention Bias Calibration (ABC)” (’24)	multi-digit arithmetic (add, parity, successor)	No	No (Fixed attention biasing)	exact-match	100% accuracy on 50-digit addition after training on 6-digit; perfect extrapolation ×8. Depends on hard-coded (unlearned) attention weights.
Looped Transformers for Length Generalization (ICLR ’25)	arithmetic (addition)	No	No position encoding in general	exact-match	Perfect only when recurrences = predetermined number of recurrent steps; degrades to 0 before and after; no autoregressive/MLM structure; supervised step count: trained on supervised shifting of input token sequence to match the correct output.
Veisi & Mansourian, “Cable” (ArXiv ’25)	language modeling (WikiText-103)	No	Yes (context-aware bias)	perplexity	Trained at 512 tokens outperforms 1024-trained baseline at 1024 tokens.

Table 2: Length-extrapolation methods on language-modeling and advanced tasks (continued).

4 Definitions

4.1 Mathematical Preliminaries

- **Relative position.** We view relative position as a *learned distance function* $d : \{0, \dots, P - 1\} \rightarrow \mathbb{R}_{\geq 0}$ that satisfies the axioms of a metric up to a global scale: $d(k, k) = 0$, $d(k, \ell) = d(\ell, k)$, $d(k, \ell) \leq d(k, m) + d(m, \ell)$. The function is anchored at an arbitrary reference token at position (or time) k whose distance starts at 0 and grows to a maximum of $P = T$ at position (or time) $k + T$. During self-attention, the query and key *position streams* supply sinusoidal position embeddings $f(d(k, \ell))$ whose inner product acts as a *similarity function*; thus learning $d(\cdot)$ end-to-end is equivalent to learning the geometry in which similarity is measured.

4.2 Relative Position as a Learned Metric Space

Every token carries a position. Let the input sequence be

$$S = \langle x_0, x_1, \dots, x_{T-1} \rangle.$$

To each index t we assign a non-negative scalar coordinate

$$z_t \in [0, P),$$

which serves as that token’s relative position in the sequence. At this introductory stage, z_t is simply a learned value that orders token x_t with respect to an implicit reference point (itself learned later). We will explain in Section 5.1 how these z_t arise from a stochastic update, but here they function only as latent “distance” values encoding each token’s place within the sequence.

4.2.1 Learned distance function (idealized definition)

Continuous view. Let $r : [0, T] \rightarrow \mathbb{R}_{\geq 0}$ be the latent *cursor trajectory* generated by the reset/increment/decrement gates in the limit of infinitesimal time steps. Define its *derivative/gradient*

$$v(t) = \frac{dr}{dt}(t)$$

and set

$$d(t, t') = \int_t^{t'} v(\tau) d\tau, \quad 0 \leq t < t' \leq T. \quad (1)$$

Equation (1) is the line integral of the instantaneous jump rate; it satisfies all metric axioms (non-negativity, identity of indiscernibles, symmetry, and the triangle inequality) up to a global scale.

Discrete Definition. Let the discrete *forward difference*

$$\Delta_t = r_{t+1} - r_t \in \{-1, 0, +1\}, \quad t \in \{0, \dots, T - 1\},$$

play the role of a one-dimensional vector field $F(t) = \Delta_t$. Because F represents a true gradient—there exists a scalar potential r_{t_0} such that $F(t) = \nabla r_t$ —its discrete line integral over any path depends only on the end points. In particular, for any $0 \leq t_0 < t_1 \leq T$,

$$\sum_{t=t_0}^{t_1-1} F(t) = \sum_{t=t_0}^{t_1-1} \Delta_t = r_{t_1} - r_{t_0}.$$

Hence the **signed displacement**

$$d_{\pm}(t_0, t') = \sum_{t=t_0}^{t'-1} \Delta_t = r_{t'} - r_{t_0}$$

is the discrete analogue of the fundamental theorem of line integrals.

In our learned metric-space formulation, we fix a learnable reference index—without loss of generality, index 0, so that r_0 is its learned coordinate. We then identify

$$z_{t_0} = r_{t_0} - r_0 = \sum_{t=0}^{t_0-1} \Delta_t,$$

which ensures that each latent coordinate z_{t_0} exactly equals the discrete “distance” (integral of Δ_t) from the reference token at index 0 up to index t_0 . In other words, z_{t_0} is the learned integral value from the reference point through all intermediate Δ_t .

5 Architectural Details

5.0.1 Dynamic origin via the reset gate.

We want relative distances of our model to be anchored to any arbitrary position in the sequence in a learnable fashion. The signed displacement $d_{\pm}(t, t') = r_{t'} - r_t$ is correct *only when the two timestamps share a common origin*—namely, the most recent position at which the reset gate fired. Let

$$\tau(t) = \max\{t_0 \leq t : \text{reset gate at } t_0 = 1\}$$

denote the last reset before or at t . We then reinterpret the cursor as a *relative coordinate*

$$\hat{r}_t = r_t - r_{\tau(t)},$$

so that $\hat{r}_{\tau(t)} = 0$ by definition. For any two points $t < t'$, the conservative-field argument yields

$$d_{\pm}(t_0, t') = \hat{r}_{t'} - \hat{r}_{t_0} = \sum_{t=t_0}^{t'-1} \Delta_t, \tag{2}$$

but (2) is meaningful *only if* $\tau(t_0) = \tau(t')$ (i.e. both points are measured relative to the same reset). Whenever $\tau(t_0) \neq \tau(t')$ —for example, if a reset occurs between t_0 and t' —the model first reanchors the origin at $r_{\tau(t')}$, yielding a piece-wise path integral whose segments are each evaluated with respect to their local origin. Refer to A.4 for reasoning behind this decision and interpretations.

5.0.2 Learned path–integral distance *distribution*.

In practice, rather than committing to a single shortest-path distance, our model treats the latent cursor trajectory $\mathcal{Z}_{k \rightarrow \ell} = (z_k, z_{k+1}, \dots, z_{\ell})$ as a *stochastic path* whose increments $\Delta_t = z_{t+1} - z_t \in \{-1, 0, +1\}$ are drawn from the Bernoulli gates described in Section 5.1. The *signed displacement* $D_{k \rightarrow \ell} = \sum_{t=k}^{\ell-1} \Delta_t$ is therefore a *path integral under uncertainty*. Formally, the probability mass at offset d is the Feynman–Kac–type functional integral over all admissible paths.

Its *probability mass function* marginalizes over *all* paths of elementary shifts. Let $\mathbf{\Delta}_{k:\ell-1} = (\Delta_k, \Delta_{k+1}, \dots, \Delta_{\ell-1}) \in \{-1, 0, +1\}^{\ell-k}$ be the sequence of elementary shifts. Then

$$\Pr(D_{k \rightarrow \ell} = d) = \sum_{\Delta_{k:\ell-1} \in \{-1,0,+1\}^{\ell-k}} \left[\prod_{t=k}^{\ell-1} p(\Delta_t | \theta_t) \right] \mathbf{1}\left\{ \sum_{t=k}^{\ell-1} \Delta_t = d \right\}. \quad (3)$$

Refinement with a dynamic origin. Whenever the reset gate (Section 5.0.1) "fires", it re-anchors the coordinate frame; any increments before that time no longer contribute to the net displacement. Introduce the reset indicator $R_t \in \{0, 1\}$, so that the effective displacement from k to ℓ is governed by

$$\Pr(D_{k \rightarrow \ell}^* = d) = \sum_{\substack{\mathbf{R}_{k:\ell-1} \in \{0,1\}^{\ell-k} \\ \Delta_{k:\ell-1} \in \{-1,0,+1\}^{\ell-k}}} \left[\prod_{t=k}^{\ell-1} p(R_t | \theta_t) p(\Delta_t | \theta_t) \right] \chi_{k,\ell}(\mathbf{R}, \Delta; d). \quad (4)$$

Here we have introduced the *path-indicator* function $\chi_{k,\ell}$, which enforces that only the increments after the last reset contribute:

$$\chi_{k,\ell}(\mathbf{R}, \Delta; d) := \mathbf{1}\left\{ \sum_{t=k}^{\ell-1} \Delta_t \prod_{u=t+1}^{\ell-1} (1 - R_u) = d \right\}. \quad (5)$$

Equation (4) reduces to (3) when $R_t = 0 \forall t$. Intuitively, each reset *excises* the history before it, so the path integral accumulates only those steps measured in the current relative frame. This refinement aligns the probabilistic distance with the geometric definition of a dynamic origin introduced in Eq. (2).

Here each block $[s_j, s_{j+1})$ contains *no* intervening reset, so the local displacement distribution inside the product is exactly the original Feynman–Kac sum. The overall distance distribution is therefore a *mixture* of block-wise integrals glued together at reset landmarks—mirroring how the model dynamically re-anchors its coordinate system whenever the reset gate fires.

5.0.3 Position Update with Copy Branch

We generalize the classic reset operation (which re-centers the relative position to a fixed origin, typically 0) by allowing a “copy” operation: at any time t , the model may *copy* its reference position from any previous position, rather than only resetting to the start. This defines a learned “constant of integration” for the position histogram update. Formally, the position update becomes:

$$\mathbf{h}_{t+1} = \mathcal{U}(\mathbf{h}_t; \mathbf{p}_{\text{reset}}, \mathbf{p}_{\text{incr}}, \mathbf{p}_{\text{decr}}, \mathbf{p}_{\text{keep}}, \mathbf{p}_{\text{copy}})$$

where \mathbf{p}_{copy} is a (possibly sparse) distribution over copy targets and a null option.

Implementation In our architecture we add a **copy branch** to the position histogram update for a subset learned learned relative position cursors, corresponding 1:1 to a subset of the query vectors in standard dot product attention. This branch enables the model, at each step, to optionally copy its reference position from any previous key (or token) position, not just reset to zero. This operation is implemented by augmenting the stochastic update matrix with a copy distribution $\mathbf{p}_{\text{copy}} \in \Delta^{P+1}$ over all candidate positions and a null (“no-copy”) option. Importantly, for the experiments in this paper, we only apply the copy branch for a subset of the tasks. Refer to Experiments (??) for more details.

5.0.4 Position Update with Copy Branch

We generalize the classic reset-only update (which always re-anchors to position 0) by adding a learned “copy” branch: at time t , the model may copy its reference position from any previous index k , instead of only resetting to 0. Concretely, let

$$\mathbf{h}_t \in \Delta^{P-1}$$

be the categorical distribution over all P possible positions at step t , and let

$$\mathbf{p}_{\text{copy}}(t) \in \Delta^P$$

be a (learned) distribution over “copy-from index” $k = 0, \dots, P - 1$ plus a terminal “no-copy” slot. Define

$$p_{\text{no-copy}}(t) = 1 - \sum_{k=0}^{P-1} p_{\text{copy}}(t, k).$$

Then the next-step histogram becomes a mixture of (1) the standard reset/incr/decr update—only if we do not copy—and (2) direct jumps into one-hot modes at each k if we do copy:

$$\mathbf{h}_{t+1} = p_{\text{no-copy}}(t) \mathcal{U}_{\text{standard}}(\mathbf{h}_t) + \sum_{k=0}^{P-1} p_{\text{copy}}(t, k) \mathbf{v}_k, \quad (3.8')$$

where:

- $\mathcal{U}_{\text{standard}}(\mathbf{h}_t) \in \Delta^{P-1}$ is the usual *reset/incr/decr/keep* update applied to \mathbf{h}_t (i.e. exactly as in Eq. (3.7) with no copy branch).
- \mathbf{v}_k denotes the one-hot vector whose only nonzero entry is at position k .
- $p_{\text{no-copy}}(t) = 1 - \sum_{k=0}^{P-1} p_{\text{copy}}(t, k)$ ensures that $\sum_{i=0}^{P-1} [\mathbf{h}_{t+1}]_i = 1$.

In other words, with probability $p_{\text{no-copy}}(t)$ we proceed exactly as in the standard histogram update, and with probability $p_{\text{copy}}(t, k)$ we force the next histogram to collapse entirely to position k . This minimal modification recovers the usual reset-only behavior when $\mathbf{p}_{\text{copy}}(t)$ is a delta at the “null” slot, but allows flexible copying from any past index when desired. See Algorithm 3 for the fully detailed implementation. In practice, $p_{\text{copy}}(t, k)$ is determined using a standard, causally masked self-attention matrix.

This generalizes the reset operation (\mathbf{p}_{copy} as a delta at 0) and allows flexible reference anchoring—crucial for dynamic tasks such as copying from arbitrary indices. See Alg. 1 for details.

5.0.5 Recurrent Neural Network Architecture

To compute for latents θ_t described in eq. 4, we implement the gating mechanism via a Gated Recurrent Unit (GRU) with a hidden state dimension of 100, whose weights are learned end-to-end alongside the rest of the model. While our architecture does not require a recurrent model to extrapolate on many (if not most) tasks, we have included it in order to reduce the number of transformer layers and to explore the usefulness of a more recurrent architecture. Furthermore, while the Histogram Update Rule is also computed sequentially, the implementation of the GRU, as well the Histogram Update Rule can be significantly parallelized in terms of overhead via kernel fusion, which we leave for future work.

5.1 Histogram Update Rule

In Section 5, we outlined the basic histogram update rule mathematically. Here we summarize the histogram update algorithm⁴. The *optimized* algorithm in pseudocode, including the 'copy branch', is detailed in Algorithm 1 of Appendix.

We then briefly analyze the computational complexity of a naive update rule implementation, followed by the complexity of our optimized approach. Note that the copy branch of the full algorithm in Appendix 1 does not increase the optimal upper bound in the computational complexity of our algorithm.

Step 1: Reset Branch.

If reset occurs, all mass flows to position 0, then is split by action:

$$\begin{aligned} \text{Total mass: } S &= \sum_{i=0}^{P-1} [\mathbf{h}_t]_i \\ \text{Reset increments: } r_{\text{inc}} &= S \cdot p_{\text{reset}}(t) \cdot p_{\text{incr}}(t) \\ \text{Reset decrements: } r_{\text{dec}} &= S \cdot p_{\text{reset}}(t) \cdot p_{\text{decr}}(t) \\ \text{Reset keep: } r_{\text{keep}} &= S \cdot p_{\text{reset}}(t) \cdot p_{\text{keep}}(t) \end{aligned}$$

The reset-branch histogram is

$$[\mathbf{h}_{t+1}^{(\text{reset})}]_i = \begin{cases} r_{\text{inc}}, & i = 1 \\ r_{\text{keep}} + r_{\text{dec}}, & i = 0 \\ 0, & \text{else} \end{cases}$$

Step 2: No-Reset Branch.

If no reset, the histogram is shifted left/right/stays according to the action probabilities:

$$\begin{aligned} [\mathbf{h}_{t+1}^{(\text{no-reset})}]_i &= [\mathbf{h}_t]_i \cdot (1 - p_{\text{reset}}(t)) \cdot p_{\text{keep}}(t) \\ &\quad + [\mathbf{h}_t]_{i-1} \cdot (1 - p_{\text{reset}}(t)) \cdot p_{\text{incr}}(t) \\ &\quad + [\mathbf{h}_t]_{i+1} \cdot (1 - p_{\text{reset}}(t)) \cdot p_{\text{decr}}(t) \end{aligned}$$

(Assume $[\mathbf{h}_t]_{-1} = [\mathbf{h}_t]_P = 0$.)

Step 3: Sum and Sharpen using the γ parameter for each cursor c .

$$\mathbf{h}_{t+1} = \mathbf{h}_{t+1}^{(\text{reset})} + \mathbf{h}_{t+1}^{(\text{no-reset})}$$

In order to prevent oversmoothing we use the power-sharpening (temperature $\gamma > 1$), then⁵:

$$\mathbf{h}_{t+1}^{(\text{sharp})}[i] = \frac{([\mathbf{h}_{t+1}]_i + \varepsilon)^\gamma}{\sum_j ([\mathbf{h}_{t+1}]_j + \varepsilon)^\gamma}$$

⁴excluding the 'copy branch' initially for simplicity

⁵See Appendix A.2 for full derivation and ablations.

5.1.1 Computational Complexity

A naïve way to model the latent position after t steps is to enumerate *all* action sequences of length t . Because reset is binary (yes/no) and the action gate⁶ is ternary (inc, dec, keep), the joint number of branches grows as

$$\underbrace{(2 \times 3)}_{\text{reset} \times \text{action}}^{t \text{ times}} = 6^t,$$

i.e. exponential in t . Maintaining an explicit categorical distribution over those paths would be prohibitive.

Efficient Evaluation Our algorithm avoids this blow-up by marginalizing *incrementally*: The stochastic matrix update below (5.1.2) updates a length- P histogram \mathbf{h}_t in $\mathcal{O}(P)$ time for each *adjacent* step $t \rightarrow t+1$. Because the model is Markovian given we know θ_t , \mathbf{h}_t already contains the *exact* marginal over *all* paths that end at step t . Therefore, for any $k < \ell$ we can reconstruct the signed-displacement distribution solely from those two histograms via a discrete cross-correlation:

$$\Pr(D_{k \rightarrow \ell} = d) = \sum_{i=0}^{P-1} \mathbf{h}_k[i] \mathbf{h}_\ell[i+d], \quad -(P-1) \leq d \leq P-1. \quad (6)$$

Intuitively, $\mathbf{h}_k[i]$ gives the probability that the cursor is at position i after all paths up to step k ; $\mathbf{h}_\ell[i+d]$ gives the probability of being at $i+d$ at step ℓ . Multiplying and summing over i integrates out the latent positions while enforcing the net displacement constraint, exactly matching the Feynman–Kac sum in Eq. (4). Thus the total cost remains $\mathcal{O}(PT)$ for the entire sequence.

5.1.2 Stochastic Matrix Formulation

The update can be compactly expressed as:

$$\mathbf{h}_{t+1} = \mathbf{h}_t^\top \mathbf{M}_t$$

where $\mathbf{M}_t \in \mathbb{R}^{P \times P}$ is a row-stochastic matrix with entries determined by the above formulas.

Block-structured transition matrix. Our update circumvents the blow-up by *marginalizing* over the branching decisions in closed form. The effect of every reset/action pair can be written as a sparse, band-diagonal block in a $P \times P$ stochastic matrix \mathbf{M}_t :

$$\mathbf{h}_{t+1} = \mathbf{h}_t^\top \mathbf{M}_t, \quad \mathbf{M}_t = \mathbf{M}_t^{\text{reset}} + \mathbf{M}_t^{\text{no-reset}},$$

where each block has only $\mathcal{O}(P)$ non-zero entries (three per row after clamping). Because we apply \mathbf{M}_t implicitly with simple `scatter_add` operations, the per-step cost is

$$\boxed{\mathcal{O}(P)},$$

rather than the $\mathcal{O}(P^2)$ dense matrix–vector multiply or the $\mathcal{O}(6^t)$ path enumeration. The full pseudocode for this update rule and matrix formulation is described in Alg. 1.

⁶omitting the copy branch for simplicity

Interpretation. Thus the histogram acts as a *compressed* representation of the full branching Bernoulli–categorical process: all 6^t trajectories are still present, but their probability mass is pooled by position. This provides an exact, differentiable update whose complexity scales linearly with the support size P and the sequence length T ($\mathcal{O}(PT)$ total), enabling practical training and inference on long sequences. This block-structure corresponds to a *non-stationary HMM*; its conditional independence assumptions also let us cast the model as a first-order linear-chain CRF conditioned on the input tokens. However, this connection to probabilistic graphical models is only drawn for intuition. We take the linear (convex) combination of possible "positions", whose coefficients are represented by h_t , via *superposition* [7] of features, i.e. *position stream* vectors. See A.3 for details.

Complexity of the "copy branch". Finally, with the addition of the copy branch defined in 5.0.4, the computation complexity remains unchanged. At each time step t , computing the "copy branch" distribution $\mathbf{p}_{\text{copy}}(t)$ via a single self-attention query against all previous keys requires one dot-product of the query vector with each of the t key vectors, followed by a softmax over t scores—i.e. $O(t) = O(T)$ work. Once $\mathbf{p}_{\text{copy}}(t)$ is available, forming the mixture in Eq. (3.8) involves (1) applying $\mathcal{U}_{\text{standard}}(\mathbf{h}_t)$, which itself is $O(P)$, scaling by $p_{\text{no-copy}}(t)$, and (2) accumulating $\sum_{k=0}^{P-1} p_{\text{copy}}(t, k) \mathbf{v}_k$, which is also $O(P)$. Therefore, the total per-step cost is

$$O(t + P) = O(\max\{P, T\}).$$

In practice one takes $P = O(T)$, so each histogram update remains $O(T)$ per time step.

5.2 From distance to *similarity*.

Given a metric $d: \{0, \dots, P-1\}^2 \rightarrow \mathbb{R}_{\geq 0}$ we define a *similarity measure*

$$\sigma(k, \ell) = \kappa(d(k, \ell)), \quad 0 \leq k, \ell < P, \quad (7)$$

where $\kappa: \mathbb{R}_{\geq 0} \rightarrow [0, 1]$ is a monotonically–decreasing kernel that satisfies $\kappa(0) = 1$ and $\kappa(r_1) > \kappa(r_2)$ whenever $r_1 < r_2$. Common choices include

Gaussian (RBF):	$\kappa_{\text{RBF}}(r) = \exp\left(-\frac{r^2}{2\lambda^2}\right)$
Laplacian:	$\kappa_{\text{Lap}}(r) = \exp\left(-\frac{r}{\lambda}\right)$
Cosine–sinusoid (used here):	$\kappa_{\text{cos}}(r) = \frac{1}{d/2} \sum_{m=0}^{d/2-1} \cos\left(\frac{r}{10000 \cdot 2^{m/d}}\right),$

with bandwidth λ or, in the sinusoidal case, a log–frequency grid identical to Transformer-style position encodings. When the encoding map $f(\cdot)$ of Section ?? satisfies nearest-neighbor properties, the inner product $\langle f(k), f(\ell) \rangle$ realizes (7) exactly, so the attention mechanism respects the metric induced by $d(k, \ell)$.

Similarity via positional *streams*. We use periodic functions to define our similarity function implementation, as they give embedding vectors that can be linearly combined using the probability distribution \mathbf{h}_t . In particular, we follow the original Transformer:⁷ let d_{pe} be the block width and

$$f_{2i}(z) = \sin\left(z e^{-\ln 10000 \cdot 2i/d_{\text{pe}}}\right), \quad f_{2i+1}(z) = \cos\left(z e^{-\ln 10000 \cdot 2i/d_{\text{pe}}}\right), \quad i = 0, \dots, \frac{d_{\text{pe}}}{2} - 1.$$

⁷`div_term` in the reference PYTORCH/NUMPY routine is $\exp(-\ln 10000 \cdot 2i/d_{\text{pe}})$.

Position stream superposition. Instead of collapsing the histogram to a single expected coordinate, we form the *position stream* $\mathbf{e}_t = \sum_{k=0}^{P-1} \mathbf{h}_t[k] f(k)$, so that *every* plausible position contributes its full encoding.

Hierarchical PE. We concatenate four such superposition features evaluated at the *same* position to obtain a length- $4d_{pe}$ embedding $g(t) = [\mathbf{e}_t^0 \parallel \mathbf{e}_t^1 \parallel \mathbf{e}_t^2 \parallel \mathbf{e}_t^3]$, or, more generally,

$$g(t) = [\mathbf{e}_t^0 \parallel \mathbf{e}_t^1 \parallel \dots \parallel \mathbf{e}_t^{C-1}] \in \mathbb{R}^{C d_{pe}}, \quad \text{where } \mathbf{e}_t^c = \sum_{k=0}^{P-1} \mathbf{h}_t^c[k] f(k), \quad c = 0, \dots, C-1.$$

which allows the model to learn coarse-to-fine spatial features. For the detailed algorithm, refer to Alg. 2.

Learned similarity. During self-attention the query and key streams interact through

$$\alpha_{h,c} \langle \mathbf{g}_t^{(q,c)}, \mathbf{g}_s^{(k,c)} \rangle, \quad (8)$$

where $s \geq t$, $\alpha_{h,c} \geq 0$ is a *learnable, head-specific* scaling coefficient. Because $\langle g(k), g(\ell) \rangle \propto \sum_{j=0}^3 \cos(\omega_{1\dots d_{pe}/2}(k^j - \ell^j))$, the similarity decays smoothly with the distance $d(k, \ell) = |k - \ell|$, yet exhibits a sharp, Gaussian-like peak at $k = \ell$ once the sum over multiple frequencies is taken—providing local precision and long-range smoothness that are crucial for reliable length extrapolation. For the detailed algorithms, refer to Alg. 3 and Alg. 4.

Notably, the sinusoidal superposition encoding $\mathbf{e}_t = \sum_j \mathbf{h}_t[j] f(j)$ maps *every coefficient of the histogram* into phase information; subsequent dot-product attention therefore receives a signal that implicitly contains *all* moments of $D_{k-\ell}$, not just its mean.

Hybrid unnormalised score. For the hierarchical positional-encoding variant we mix the standard dot-product term with the learned similarity term to obtain the head-wise unnormalised self-attention score

$$\tilde{a}_{t,s}^{(h)} = \mu^{(h)} \langle \mathbf{q}_t^{(h)}, \mathbf{k}_s^{(h)} \rangle + (1 - \mu^{(h)}) \alpha_{h,c} \langle \mathbf{g}_t^{(q,c)}, \mathbf{g}_s^{(k,c)} \rangle, \quad \mu^{(h)} \in [0, 1], \quad (9)$$

where μ (learned per head) gates between the conventional self-attention score and the frequency-based learned similarity from Section 5.2. Setting $\mu = 1$ recovers vanilla self-attention, whereas $\mu = 0$ relies purely on the hierarchical positional signal; learning μ allows the model to interpolate continuously between the two.

6 Experiments

Task suite overview. Table 3 - Table 4 summarize the eight self-supervised problems that constitute our benchmark. All of them share one crucial property: **only the tokens to the right of the “=” sign are supervised, so the model must learn to read the left side and predict the completion.** We only measure exact-match accuracy; therefore, all tokens, including chain-of-thought tokens, must be predicted correctly in order for the answer to be marked correct. Furthermore, we require all end of sequence (EOS) tokens to be outputted in order for the model’s answer to be marked correct. The tasks span arithmetic (Addition, Multiplication), list processing (Reverse, Odds First), stack semantics, program-like navigation (SCAN-CoT), and two forms of string copying, thereby exercising both symbolic and positional generalization.

SCAN-CoT expansion. Because **SCAN-CoT** is derived 1:1 from a fixed-dataset of only $\sim 20k$ unique examples via chain-of-thought tokens, we visualize its length distribution in Appendix D. For stratifying results, we measure accuracies on the entire test set, All train/test examples are derived 1:1 with the originals by expanding the correct output tokens via the chain-of-thought tokens described in Table 4.

Multiplication CoT expansion. In our chain-of-thought representation of $a \times b$, we unfold the standard grade-school long-multiplication via the distributive law:

$$a \times b = a \times \left[\sum_i d_i \times 10^{p_i} \right] = \sum_i (a \times d_i) \times 10^{p_i}.$$

Here each digit d_i of the multiplier b produces a partial product $a \times d_i$, and is then shifted by p_i places (i.e. padded with p_i zeros) according to its place value. We annotate each term as

$$d_i (d_i \rightarrow p_i)$$

to indicate that the partial product $a \times d_i$ is followed by p_i zeros. This sequence of weighted, place-shifted multiplications fully encodes the long-multiplication algorithm, without ever performing the final addition. The correct output tokens via chain-of-thought is described in Table 4.

6.0.1 Copy-branch ablation.

Our histogram encoder can optionally perform a 'copy branch' jump (§ 5.0.3) via a dedicated branch. We toggled this feature per experiment as listed below:

For Addition, Odds First, Stack Manipulation, and CoT-only Multiplication the copy branch was *disabled* on every head.

For Reverse, SCAN-CoT, and dyn_str_cpy, the **copy branch** was *enabled* on a small subset—one out of every five query cursors. For the corresponding key cursors, from which query could perform a copy branch operation, the corresponding key cursor histogram was fixed to increment-only, so that the relative positions corresponded to exactly to the corresponding tokens' **absolute** instead of learnable relative positions. We emphasize the generality of this approach to other text retrieval tasks in practice, because for a small fraction of our position encodings, it is useful to allow our model to make them absolute rather than relative positions, so as to give each token a *unique* position encoding. Therefore, some of our query vectors are *guaranteed* to be able to attend to each past token uniquely.

Empirically, with the exception of **SCAN** and **dyn_str_cpy** we observed no extrapolation difference when that key cursor was allowed to train, but we keep the setting fixed for consistency. All other experiments also ran with the copy branch turned off.

Table 3: Self-supervised tasks used in our experiments. Only the tokens **to the right of the “=” sign** are optimized.

Task	Input prefix (left of “=”)	Target completion (right of “=”)	Example
Addition	Two integers written least-significant-digit first, separated by “+”, then “=”.	Comma-separated chain-of-thought; each step emits the four per-digit tokens $\langle d_a, d_b, c_{out}, d \rangle$ (addend a digit, addend b digit, outgoing carry, result digit). After the list we write “→” followed by the reversed sum and a final “.”. The answer is marked correct only when **all** CoT steps <i>and</i> the final digits are correct.	8 2 9 + 0 3 = 8 0 0 8 , 2 3 0 5 , 9 0 0 9 → 8 5 9 .
Copy	Random digit sequence.	Identical sequence.	8349216=8349216.
Reverse	Random digit sequence.	Sequence reversed.	8349216=6129438.
Odds First	Length- L digit sequence over $\{0, \dots, V - 1\}$.	Digits at odd indices (1-based) concatenated in order, then the even-indexed digits.	012345=135024.
Stack Manipulation	Initial binary stack (0/1 written bottom→top) followed by actions {2: POP, 3: PUSH 0, 4: PUSH 1}; total length ℓ , then “=”.	Resulting stack written <i>top-to-bottom</i> , a terminator “2”, and zero-padding to reach length $\ell + 1$.	0 1 1 0 4 2 2 = 1 1 0 2 0 0 0 0.

Table 4: Self-supervised tasks used in our experiments (Continued). Only the tokens **to the right of the “=” sign** are optimized.

Task	Input prefix (left of “=”)	Target completion (right of “=”)	Example
SCAN-CoT ⁸	All train/test data are obtained by converting the full <i>length-split</i> split of SCAN into chain-of-thought form.	Chain-of-thought for every sub-clause, followed by “→”, then <i>all</i> low-level action tokens. The model must predict the full CoT, not just the final actions.	walk around left thrice and look opposite right = walk around left + walk around left + walk around left and look opposite right → walk around left : I_TURN_LEFT I_WALK I_TURN_LEFT I_WALK I_TURN_LEFT I_WALK I_TURN_LEFT I_WALK walk around left : I_TURN_LEFT I_WALK I_TURN_LEFT I_WALK I_TURN_LEFT I_WALK walk around left : I_TURN_LEFT I_WALK I_TURN_LEFT I_WALK I_TURN_LEFT I_WALK walk around left : I_TURN_LEFT I_WALK I_TURN_LEFT I_WALK I_TURN_LEFT I_WALK look opposite right : I_TURN_RIGHT I_TURN_RIGHT I_LOOK . 5839472,3=39472.
dyn_str_cpy	Pair “ s, d ” where d occurs exactly once in s .	Substring of s starting at that unique d , where the start index $t \sim \text{Uniform}(\{1, \dots, n\})$, $n = s $	
Integer-Multiplication (CoT only)	“ $a \times b =$ ”.	so output s_t . Program-like CoT string that rewrites $a \times b$ as $a \times [\textit{weighted digit mappings}]$; the final product is <i>not</i> required.	675x1259= 675x[1*(1+1)(2+0)(5+0)(9+0)+2*(2+1)(5+0)(9+0)+5*(5+1)(9+0)+9*(9+1)].

⁸Adapted directly from the SCAN [14] *length-split* corpus (<https://github.com/brendenlake/SCAN/tree/>)

6.1 Evaluation Protocol

All models are evaluated every 1,000 training steps (after crossing a loss threshold of 0.1) on a held-out test set of 1,000 examples. For each evaluation point we record the accuracy, and in our final plots report the average of the *top* three accuracies attained across training. In Figures 1–10, individual sample points (at each 1k step) are marked explicitly, and the dashed bands indicate a $\pm 10\%$ margin around the line.

6.2 Model Architectures

Tokenization All models use per-digit tokenization and a vocab size of 64 across all tasks. On all tasks, the full vocab is not used but is kept constant.

Baseline Transformer. As a reference, our baseline is a standard 5-layer Transformer (Vaswani *et al.* 2017) with sinusoidal absolute position encodings, 8 heads per layer, weight-tied unembeddings with the input vocab embeddings, and an embedding dimension of 512. We also use *randomly shifted APE position encodings* [17] to allow the model to make use of all position embeddings.

Choosing a Representative Baseline for this Working Paper. Recent studies have consistently shown that a small number of positional-encoding schemes capture the bulk of length-extrapolation behavior in compact transformer models. In particular, [22] demonstrated that randomized positional encodings (RPE) match or exceed the extrapolation accuracy of absolute positional encodings (APE) on a variety of synthetic sequence tasks. McLeish *et al.* [17] further showed that “Abacus” embeddings enable arithmetic transformers to generalize far beyond their training lengths with minimal modifications. Kazemnejad *et al.* [13] conducted a broad comparison across multiple encoding families and found that, once hyperparameters are tuned, most alternatives perform on par with APE. Finally, Saxton *et al.* [23] analyzed arithmetic reasoning in small transformers and observed that augmenting APE with lightweight task-specific tweaks yields nearly identical length-extrapolation trends. Taken together, these convergent results justify our focus on APE as a single representative baseline; we note, however, that an expanded empirical comparison—including RPE, Abacus, and other leading schemes—is underway and will appear in an upcoming revision.

PRISM + Transformer. We augment the vanilla transformer baseline with our PRISM layer(s) as follows:

- **All tasks except Odds First and Stack Manipulation:** a single PRISM layer is inserted *before* the first Transformer layer.
- **Odds First and Stack Manipulation:** two PRISM layers are used, one before layer,1 and one before layer,4.
- Remove the absolute position encoding by decoupling the APE from the content embedding residual stream, which partially draws inspiration from the disentanglement from [10], except that we formally take the superposition of *all* residual stream [20] position encoding vectors via concatenation and linear combination.

`master/length_split`); the original command is expanded into two supervised chain-of-thought steps.

- Unless otherwise noted, the total number of *Histogram and corresponding superposition-PE Cursors* is set to 140, with $c=4$ cursors and key, query pairs per head. Refer to Section 5.2 for details.

In all cases the sinusoidal superposition embedding dimension is 340, the token–vocabulary embedding dimension is 192, and the Transformer has 5 layers.

6.3 Regularization

For all tasks (unless otherwise noted), we enforce orthogonality on the GRU hidden-to-hidden matrix W_{hh} via one of:

- PyTorch parametrization: `from torch.nn.utils.parametrizations import orthogonal,`
or
- an explicit Frobenius-norm regularizer of weight 10^{-3} on W_{hh} .

6.4 Training details

The PRISM architecture is trained with AdamW ($\beta_1=0.9, \beta_2=0.98$), for a maximum of 150k steps to a peak LR of 9×10^{-5} , batch size 100, sequence length capped at 2048 tokens (padding where necessary). All baselines are trained for 150k steps with a batch size of 100, unless otherwise noted. Across all tasks, we warm up using the minimum sequence lengths (up to length 5) for 5 k steps, then train using a maximum sequence length of 10 for the next 5 k steps. **On Stack Manipulation, Reverse, Odds First, and CoT Addition we increase the maximum sequence length in steps of 10, allocating 10 k steps to each length bucket.** For the α coefficients (§ 5.2) of our relative position cursors we use a separate AdamW group ($\beta_1=0.8, \beta_2=0.92, lr=0.03$).

7 Results

All charts follow the Experimental setup (Section 6) and use the average-of-top-3 sampling method for reporting accuracies. Unless otherwise stated, dashed vertical lines represent the maximum training distribution for each graph.

^{8*} In subsequent ablations we found that normalizing the Frobenius norm of W_{hh} to be a fixed multiple of a small learnable constant further improved extrapolation on Odds First, SCAN, and (in preliminary experiments) most other tasks.

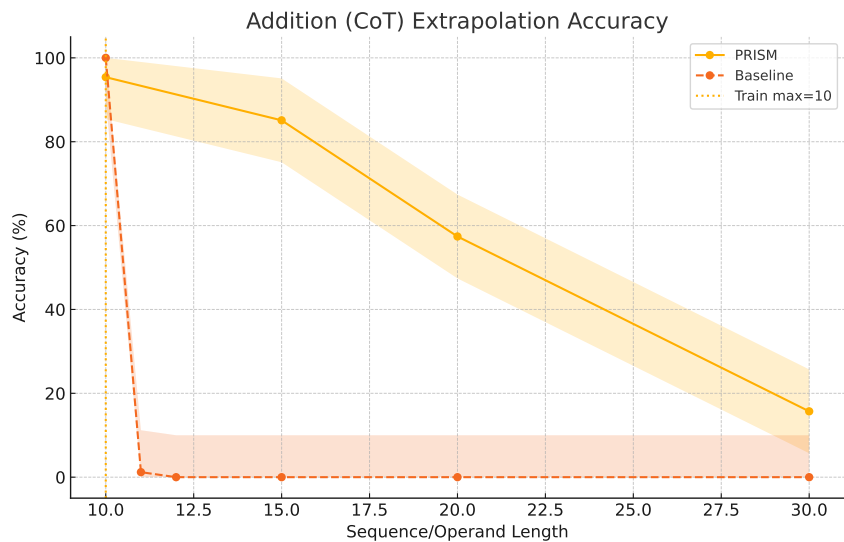


Figure 1: Addition (CoT) extrapolation accuracy. PRISM vs. Baseline. Dashed line marks the training max length (10).

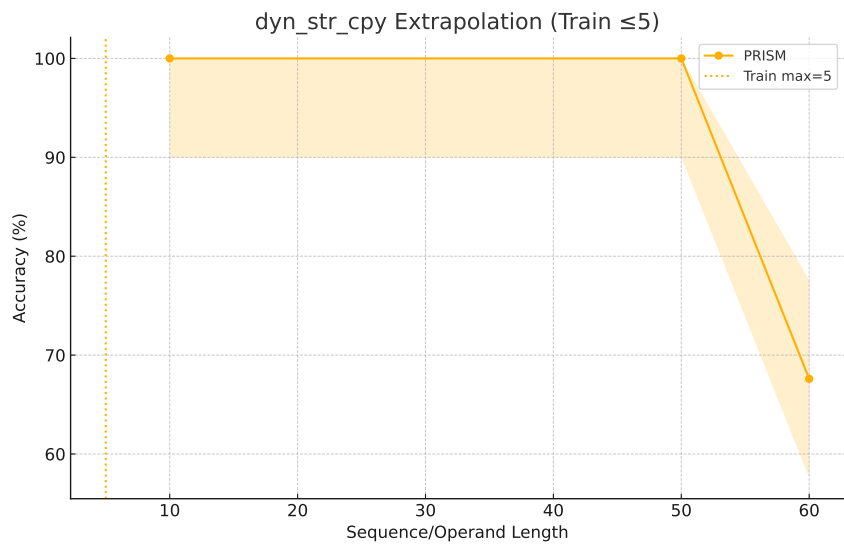


Figure 2: dyn_str_cpy extrapolation when trained up to length 5 (PRISM only).

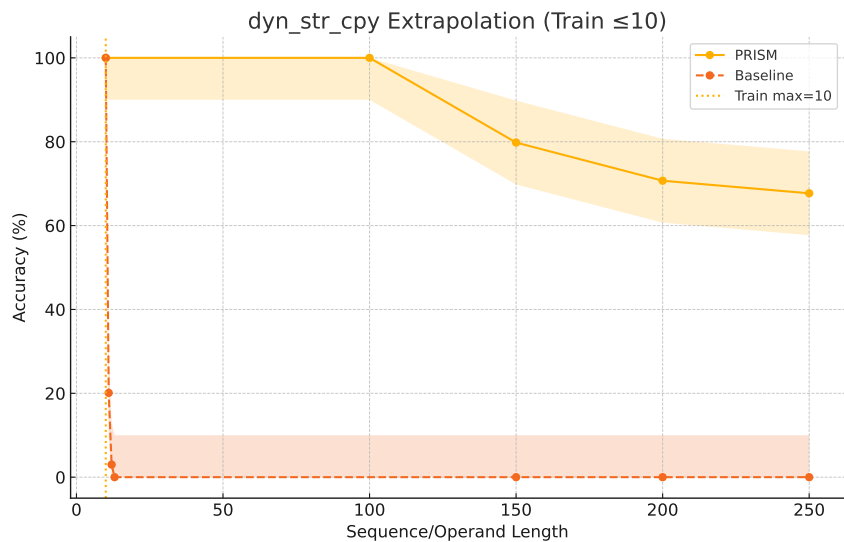


Figure 3: dyn_str_cpy extrapolation when trained up to length 10. PRISM vs. Baseline. Dashed line marks the training max length (10).

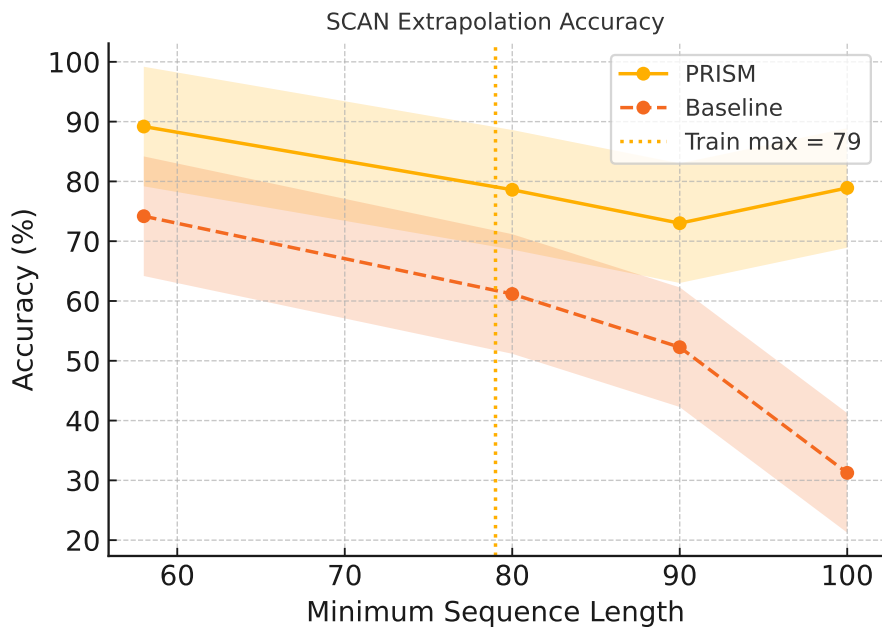


Figure 4: SCAN-CoT extrapolation accuracy for test dataset. Refer to Appendix D for length distributions of train and test sets.

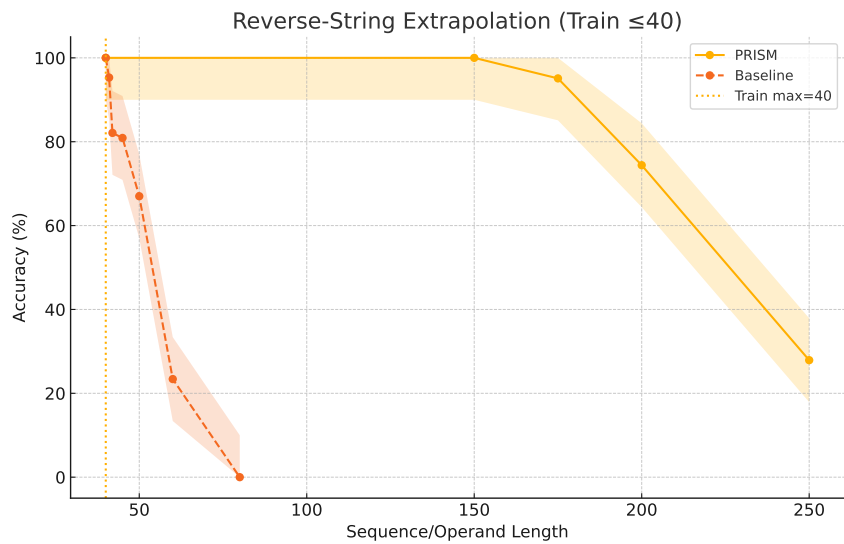


Figure 5: Reverse-String extrapolation for max-train length 40: PRISM vs. Baseline.

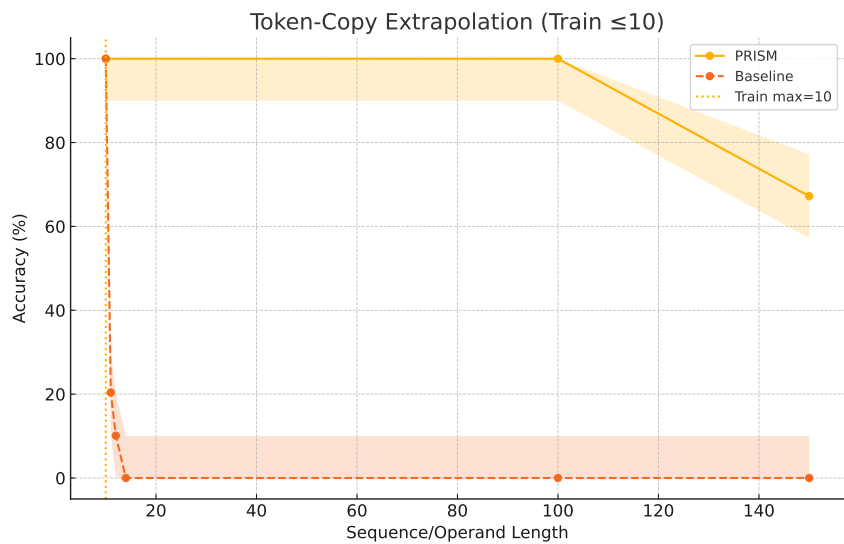


Figure 6: Token-Copy extrapolation when trained up to length 10: PRISM vs. Baseline.

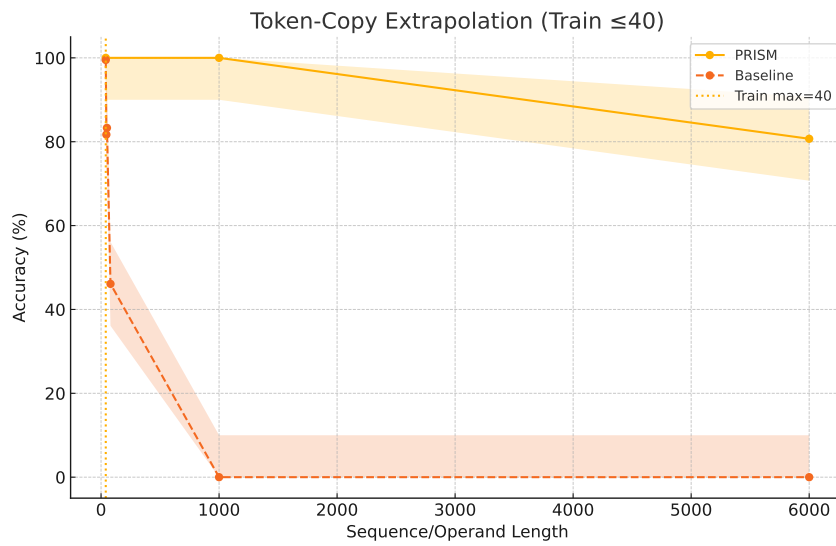


Figure 7: Token-Copy extrapolation when trained up to length 40: PRISM vs. Baseline.

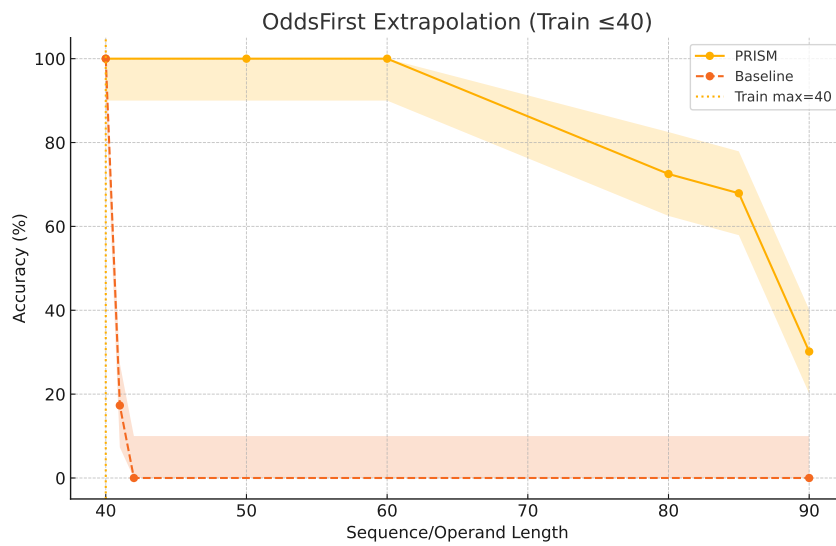


Figure 8: Odds First extrapolation accuracy for max-train length 40: PRISM vs. Baseline.

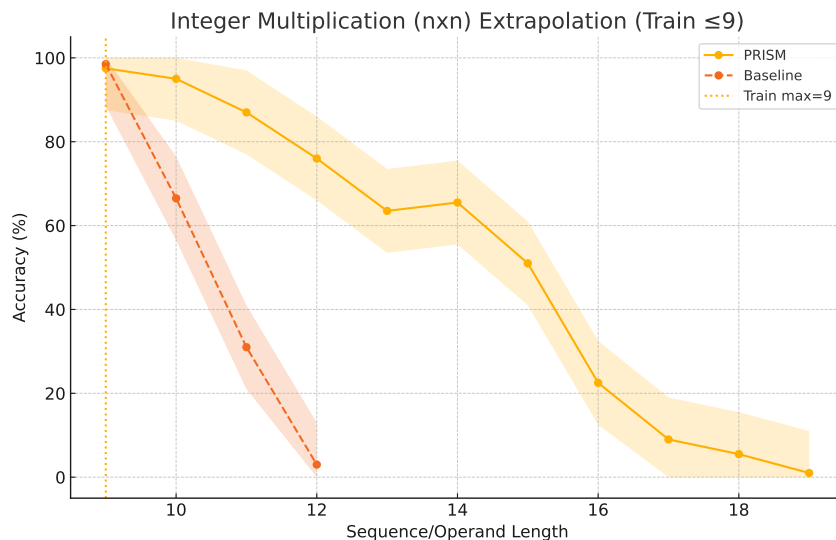


Figure 9: Integer Multiplication CoT (nxn) extrapolation for operand length up to 9: PRISM vs. Baseline. Dashed line marks the training max length (9).

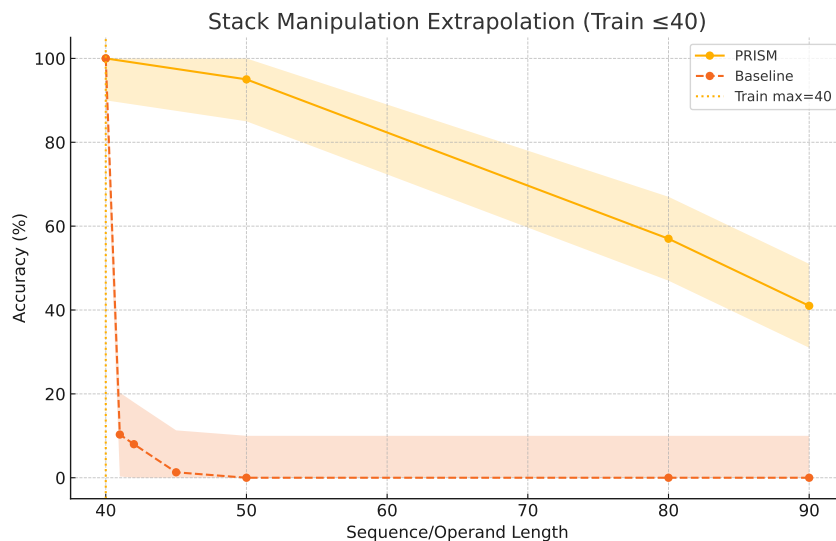


Figure 10: Stack Manipulation extrapolation for max-train length 40: PRISM vs. Baseline.

8 Discussion

We start from the empirically validated view [13, 31, 5, 3, 2, 9, 22, 17] that a wide range of simple and important skills, requiring *algorithmic* or *long-context* reasoning traces, may be set back by the limitations of existing neural network architectures. These tasks are easy for humans to learn via generalizing from observations of correct examples, so that they (a) can execute the same tasks

except where the time horizon extends beyond that observed during training, and (b) execute tasks via *compositionality* - chaining together very basic rules as the building blocks of a more complex task. In this paper, we have focused on both forms of generalization for neural networks via training them to learn from self-supervised data.

The limited *length generalization* on simple tasks that are otherwise the same as learned during training, except extended beyond the training horizon - which are limitations demonstrated by transformer, recurrent, and other sequence-to-sequence architectures - motivates this work.

Before a model can execute complex, practical tasks beyond the training horizon, and do so *reliably* and *autonomously*, the model must first have the ability to execute simpler tasks or algorithms. Practical, complex tasks include programming, software design, software modification, planning, mathematical proofs. We reiterate that what they all have in common is compositional reasoning, i.e. **applying the same basic rules and subroutines** that the model has learned in order to break down any complicated task [5] into simpler steps [14]. Fundamentally, these simpler steps require **length generalization** of the language model if the time horizon is increased beyond the training distribution.

Our experiments confirm that the proposed relative-position stream extrapolates far beyond the training length on tasks that defeat standard Transformer baselines—e.g. 20-digit chain-of-thought addition after training on only 10 digits, or copying/reversing 100-token strings after seeing 10-token examples. These findings support our long-term goal of *sequence-length generalization* for language-model reasoning.

Inspired by the view that scaling up the reliability of LLMs requires learning from data (i.e. self-supervision) [24] and from the agent’s own experiences - to the best of our knowledge - we are first to demonstrate length generalization on a variety of simple algorithmic reasoning tasks, like addition via chain-of-thought, using a purely *self-supervised approach*, meaning that our model can, in principle, learn the same tasks from a text corpus without the use of hand-crafted labels or other forms of supervised learning. Notably, other architectures trained using self-supervision have previously been noted to fail to extrapolate altogether, even via chain-of-thought prompting or other scratchpads - necessitating approaches like providing *index hints* during training and inference.

Demonstrating the understanding of simple algorithms by tracing all of their *required steps*, such as via our Chain-of-Thought Addition task, establishes confidence that **arbitrary, more complex algorithms** may be generalized beyond the training horizon. For example, algorithms are, in general, similarly unbounded in their length and memory requirements, just as an algorithm that computes the sum of two numbers can be arbitrarily complex with respect to the amount of computation steps required. Thus, when understanding *any* algorithm it has never seen before, an AI system needs to perform a sequence of operations described by a set of instructions. Thus, we view length extrapolation on the simple algorithms explored in this paper as prerequisites to extrapolation on not only more complicated forms of *algorithmic reasoning*, like graph traversal, but also tasks including software engineering & algorithm design (computer science research), systematically resolving interdependencies when building a software package (dev-ops), and in general, any task that can be broken down into simpler steps in order to describe a **correct reasoning trace** or **plan of how to execute the task**.

Because of the above and PRISM’s general-purpose architecture, which can be added to any trans-

former layer, we view our achievements as a stepping stone to models reliably transcending the training horizon on practical tasks.

9 Future Work

Aside from long-context tasks involving *sequential data* - a model should also be able to perform reasoning involving other modalities, such as graphs (e.g. a network of roads, tree-structured data), diagrams (e.g. UML, concept maps), spatial reasoning, and visual flow charts. While tasks involving these modalities similarly involve the step-by-step execution of a plan, the observations are not sequential in general.

However, due to the understanding of the spatial structure of the data that our neural architecture has demonstrated, we leave the exploration of tasks that involve the understanding of these general modalities for future work.

A Briefly Justifying Architectural Design Decisions

A.1 Why not “index hints” or similar, programmed solutions?

Prior methods such as *Abacus Embeddings*, *Inductive Scratchpads*, and related works attach fixed, one-hot embeddings at special positions (digit boundaries, start/end tokens, etc.), effectively implementing a *predetermined* counting-based *reset* scheme in a hard-coded, monotonically increasing fashion. Because the landmarks are *not learned*, these schemes do not induce a distance metric nor a similarity function: attention fires only when the two tokens carry the *exact same* hint, ignoring intermediate positions and weakening generalization once the presence of hard-coded features, sequence, or the copy-window length change. Consequently they isolate the “correct” token by construction but do not learn a genuine *relative position encoding* that satisfies the semantics of a distance metric. Such hard-coded features boost in-distribution accuracy on short, template-like tasks, yet they break down on compositional or chain-of-thought settings and cannot generalize once the latent layout differs from the hand-coded pattern. In contrast, our model learns the metric $d(\cdot)$ and its similarity map directly from data through the stochastic histogram update, enabling smooth extrapolation without manual anchors.

Our approach achieves this by *learning* both the metric d and the coefficients of the sinusoidal embedding inner product when computing the unnormalized attention matrix, allowing smooth, data-driven extrapolation to sequences far longer than those observed during training.

A.2 Sum and Sharpen using the γ parameter.

To counteract the exponential damping of confident local gates (e.g. $0.99^{50} \approx 0.60$ after 50 steps), we apply a *power-sharpening* nonlinearity described in 5.1:

$$\mathbf{h}_{t+1}^{(\text{sharp}, c)}[i] = \frac{([\mathbf{h}_{t+1}^{(c)}]_i + \varepsilon)^{\gamma_c}}{\sum_j ([\mathbf{h}_{t+1}^{(c)}]_j + \varepsilon)^{\gamma_c}},$$

where each cursor histogram c has its own learnable exponent γ_c , initialized to 2.0 at model creation.

A.2.1 Markov-kernel perspective on the ‘‘cohesion’’ effect of γ .

Equivalently, each sharpen-then-renormalize step can be seen as applying a reweighted one-step transition matrix with temperature $\tau_c = 1/\gamma_c < 1$. Over multiple timesteps this amounts to repeated exponentiation of the same stationary kernel, sharpening high-probability transitions and thereby promoting ‘‘cohesion’’ rather than diffusion.

Proof. We prove by induction on n that for a fixed sharpening exponent γ_c ,

$$p_n(i) = \frac{p_0(i)\gamma_c^n}{\sum_j p_0(j)\gamma_c^n},$$

where each update is

$$p_{t+1}(i) = \frac{p_t(i)^{\gamma_c}}{\sum_j p_t(j)^{\gamma_c}}.$$

Base case ($n = 0$). Since $\gamma_c^0 = 1$,

$$\frac{p_0(i)\gamma_c^0}{\sum_j p_0(j)\gamma_c^0} = \frac{p_0(i)}{\sum_j p_0(j)} = p_0(i),$$

because p_0 is already normalized.

Inductive step. Assume the claim holds for $n = k$, and let

$$S_k = \sum_{\ell} p_0(\ell)\gamma_c^k, \quad p_k(i) = \frac{p_0(i)\gamma_c^k}{S_k}.$$

Then

$$p_{k+1}(i) = \frac{p_k(i)^{\gamma_c}}{\sum_j p_k(j)^{\gamma_c}} = \frac{\left(\frac{p_0(i)\gamma_c^k}{S_k}\right)^{\gamma_c}}{\sum_j \left(\frac{p_0(j)\gamma_c^k}{S_k}\right)^{\gamma_c}} = \frac{p_0(i)\gamma_c^{k+1}/S_k^{\gamma_c}}{\sum_j p_0(j)\gamma_c^{k+1}/S_k^{\gamma_c}} = \frac{p_0(i)\gamma_c^{k+1}}{\sum_j p_0(j)\gamma_c^{k+1}},$$

completing the induction.

Thus after n repeated sharpenings, the original distribution’s exponents have accumulated to γ_c^n , rigorously capturing the ‘‘cohesion’’ effect. \square

A.3 Separate ‘‘Position Stream’’ and Linear Combinations of *Sinusoidal Position Encoding*

Crucially, instead of a probabilistic mixture distribution, the ‘‘probability distribution’’ represented by our histogram (5.1) h_t is more correctly interpreted as the coefficients of a linear (convex) combination of sinusoidal PEs at each time-step. This is in the same way that the self-attention mechanism of [26] takes the convex combination of value vectors. Therefore, in practice, we represent the ‘‘posterior distribution’’ over relative positions \mathbf{h}_t as a superposition of **sinusoidal positional encoding vectors**.

In other words, for a vector dimension d_{model} and position index $k \in \{0, \dots, P-1\}$, we use the “Transformer-classic” encoding introduced from [26]. Averaging scalars would erase phase information that these encodings need for dot-product attention. Indeed, for any frequency ω_m in the basis, the similarity between two positions satisfies

$$\langle f_{\omega_m}(k), f_{\omega_m}(\ell) \rangle = \cos(\omega_m(k - \ell)),$$

which *decays smoothly* as the relative distance $d(k, \ell) = |k - \ell|$ grows, while exhibiting a sharp, Gaussian-like peak at $k = \ell$ when the sum over multiple frequencies is taken. This graceful fall-off provides fine spatial resolution locally and coarse invariance at larger offsets—crucial for robust long-context reasoning.

Superposition and Relative Position Encoding Let $f : \{0, \dots, P-1\} \rightarrow \mathbb{R}^d$ be the sinusoidal position encoding and let $\mathbf{h}_t[k]$ denote the *probability* that the latent cursor is at position k after step t . We represent the uncertainty by a *superposition* of encoding vectors,

$$\mathbf{e}_t = \sum_{k=0}^{P-1} \mathbf{h}_t[k] f(k) \in \mathbb{R}^d. \quad (10)$$

Why not average scalars first? Suppose one tried to turn the histogram into a single *expected position* $\bar{k}_t = \sum_k k \mathbf{h}_t[k]$ and then feed $f(\bar{k}_t)$ downstream. Because $f(\cdot)$ is *non-linear* (component-wise sinusoid or MLP),

$$f(\bar{k}_t) \neq \sum_k \mathbf{h}_t[k] f(k) \quad \text{in general.}$$

The mismatch is severe in high-frequency dimensions. For the sinusoidal encoder $f_{2m}(k) = \sin(\omega_m k)$, $f_{2m+1}(k) = \cos(\omega_m k)$, we have

$$\begin{aligned} f_{2m}(\bar{k}_t) = \sin(\omega_m \bar{k}_t) & \quad \text{vs.} \quad \sum_k \mathbf{h}_t[k] \sin(\omega_m k) = \Im\{\mathcal{F}_{\omega_m}[\mathbf{h}_t]\}, \\ f_{2m+1}(\bar{k}_t) = \cos(\omega_m \bar{k}_t) & \quad \text{vs.} \quad \sum_k \mathbf{h}_t[k] \cos(\omega_m k) = \Re\{\mathcal{F}_{\omega_m}[\mathbf{h}_t]\}, \end{aligned}$$

where \mathcal{F}_{ω_m} is the discrete Fourier coefficient at frequency ω_m .

The Fourier transform of *the whole histogram* appears on the right-hand side, whereas the left collapses everything to one phase. Consequently, averaging positions destroys interference patterns that are crucial for attention to disambiguate periodic cues (e.g. copy-tasks, music, code indentation).

Summary Equation (10) ensures that every plausible position contributes its *full* encoding, weighted by its probability. The model can therefore *adaptively focus* on sharp or diffuse spatial hypotheses simply by modulating \mathbf{h}_t , *without* any change to the downstream attention mechanism. This maintains expressiveness while retaining the $\mathcal{O}(P)$ update cost established in Section 5.1.1.

A.4 Reset Transition - Additional Justifications

The reset gate (4) *precedes* increment/decrement, matching human procedural reasoning (“Assign a distance function relative to the left-most digit”) and avoids mutually-exclusive gate assumptions that impede training when both inc and dec are plausible.

Higher-dimensional interpretation. Another interpretation is that in 2 and higher dimensions, a reset at some (spatial) position \mathbf{t} corresponds to centering the *coordinate frame* (and setting the distance function $d = 0$) at a landmark at location \mathbf{t} , allowing the relative distance from the landmark to be correctly computed (similarly via a learned distance field) by path-integrating its gradient.

In other words for \mathbb{R}^n ($n > 1$), a reset at spatial landmark $\mathbf{t} \in \mathbb{R}^n$ sets the scalar potential $\phi(\mathbf{x})$ to zero at $\mathbf{x} = \mathbf{t}$. The reset gate therefore *dynamically centers the coordinate frame*, ensuring that the learned distance function behaves consistently—preventing scenarios (e.g. repeated landmarks) where a naïve difference $r_{t'} - r_t$ would be ill-defined.

A.5 Summary

- Collectively, these inductive biases generalize classic discrete state Markov models: the transition matrix is parameterized by learnable gate probabilities at each step.
- We can view the model as a *linear-chain conditional random field* (CRF) whose edge potentials are produced by the neural gates.
- The forward messages are updated in Eq. (5.1) via a sparse matrix–vector multiply that costs only $\mathcal{O}(P)$, instead of the naive $\mathcal{O}(P^2)$ required by a dense transition matrix.
- The model’s state at each time/position t is a categorical distribution over *relative* positions $\mathbf{h}_t^{(c)}$, rather than a single scalar or one-hot.
- The categorical distribution $\mathbf{h}_t^{(c)}$ at each timestep is a vector of coefficients for the *convex combination* of position encoding vectors.
- In particular, this convex combination emits a position encoding vector \mathbf{e}_t^c via multiplying the categorical distribution vector $\mathbf{h}_t^{(c)}$ with the standard APE⁹ matrix from [26] at each timestep/position t .
- This emitted (linearly combined) PE vector \mathbf{e}_t^c is then assigned to a unique orthogonal subspace of the *position stream*, where this orthogonal subspace is uniquely determined via *concatenation* according to the cursor index c of the histogram $\mathbf{h}_t^{(c)}$; this step is described in 7.
- The update resembles a generalized Bernoulli trial at each step, but with non-exclusive, learned gate activations.
- Although our only focus is extrapolation, we take inspiration from [18] for learning a signed distance field, which can then be integrated. Their work generalized well on *interpolation* for view synthesis between sampling points where later work [25] has shown that sinusoidal position encodings for the observation kernel have allowed for higher frequency features to be accurately learned for reconstruction.

⁹Importantly, despite the use of an "APE" table, all emitted PE vectors for our learned model represent *relative position*.

B Interpretability Visualizations

In this appendix we delve into the internal representations that PRISM learns in order to achieve robust length extrapolation. We begin by showing the gate-probability distributions at initialization and after training (Figures 11-12), which reveal how the model comes to favor incremental cursor movements over resets or decrements. Next, we visualize the *mode* of the learned positional histogram (the top-1 most likely offset) for each task, both at the start of training and at convergence (Figures 13-15), to demonstrate how PRISM sharpens its beliefs about relative positions. We include out-of-distribution (OOD) histograms for the addition and reverse tasks (Figures 16-20) to show that these learned distributions remain coherent far beyond the training horizon. Finally, we display the self-attention masks that emerge on the reverse task (19, 20) and compare against a randomized-PE baseline (18), highlighting how our differentially learned encodings outperform fixed or random schemes.

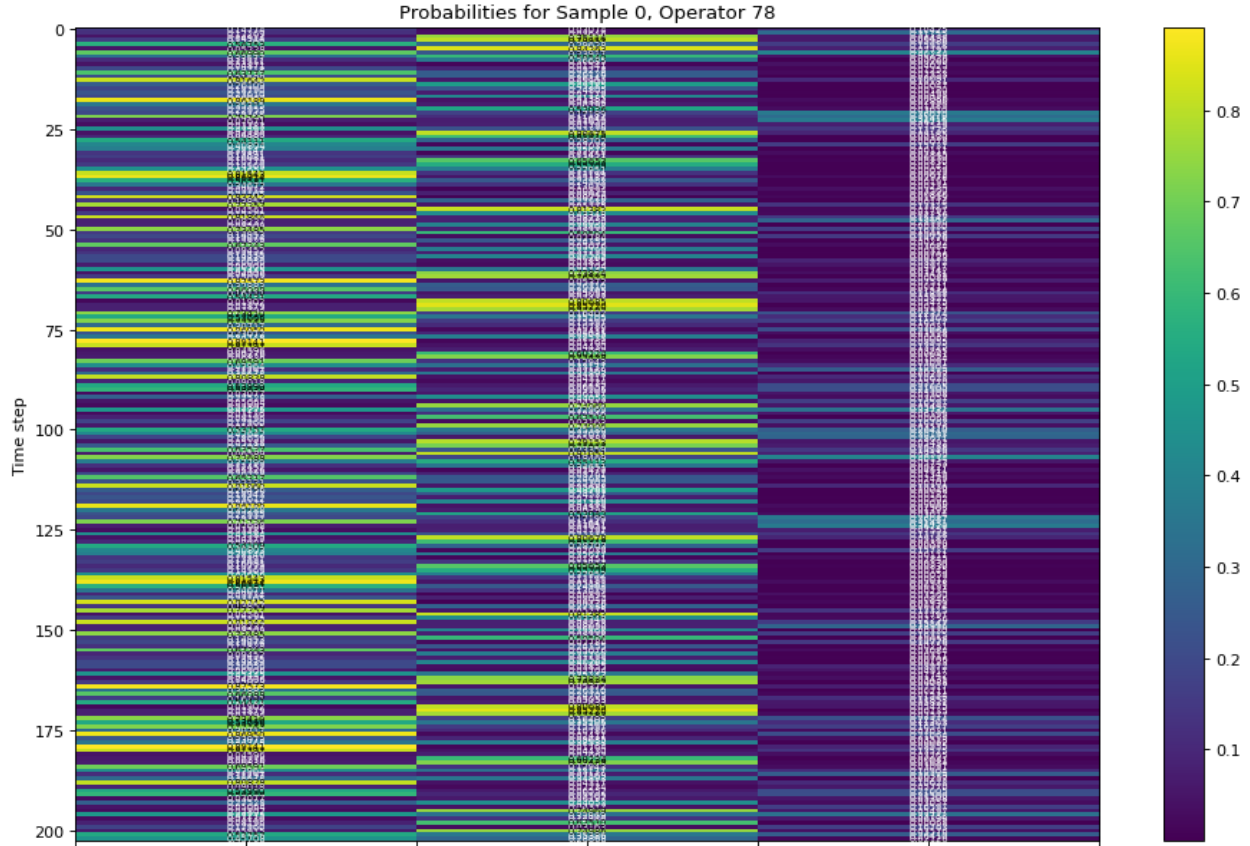


Figure 11: Gate probability distributions at initialization. Each PRISM cursor starts with uniform priors over the four actions—increment, decrement¹¹, and reset—reflecting maximal initial uncertainty about position updates. Columns from left to right correspond to increment, decrement, reset, respectively, for the histogram probabilities at each position defined in 4.

¹¹“Keep” probabilities are implicitly represented here as $1 - (p_{\text{inc}} + p_{\text{dec}})$.

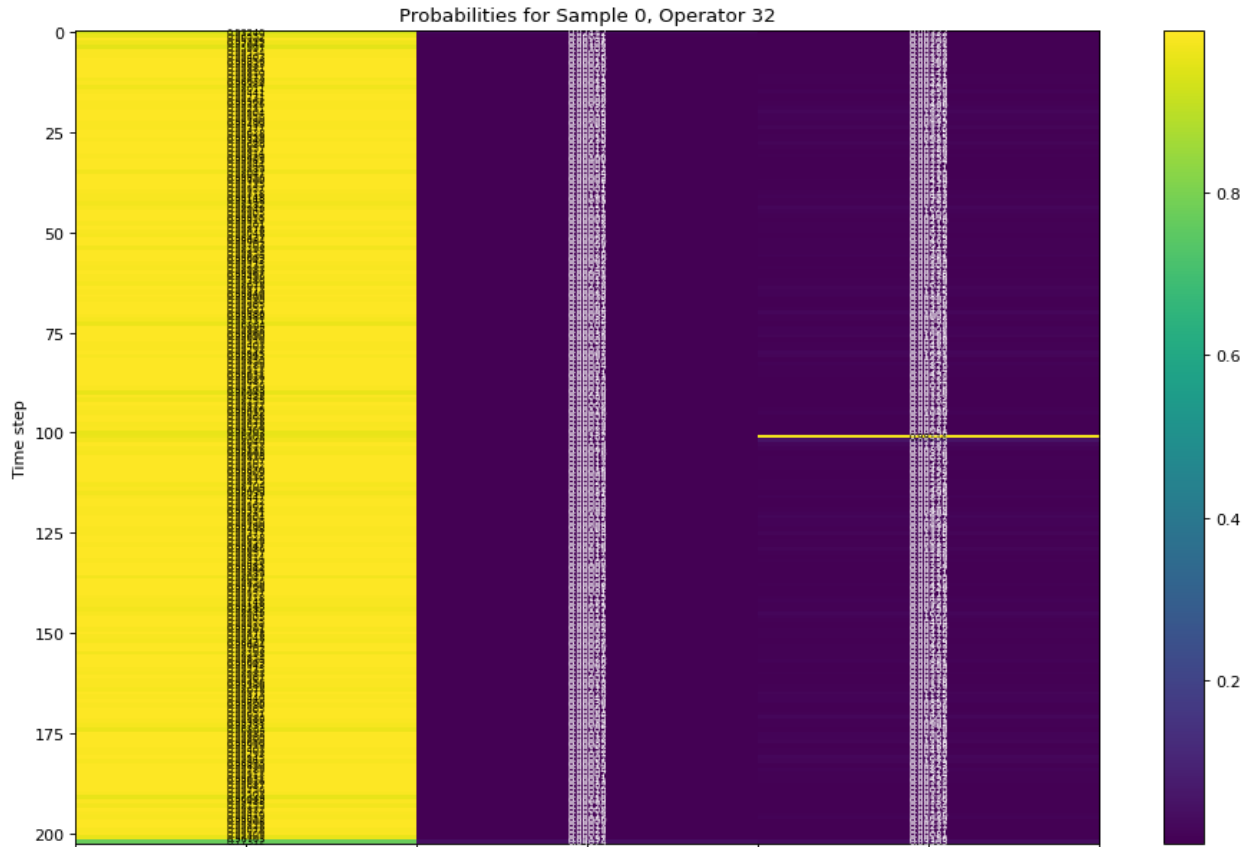


Figure 12: Learned gate probability distributions after training on token-copy. PRISM develops a strong bias toward *increment* actions, with resets and decrements used sparingly, enabling smooth advancement of the internal cursor across long sequences.

Graph 2, Latest Cached Real Positions for fixed_output_gates = False, fixed_reset_gates = False, range = range(0, 75), RE/layer num = 0, first_half = True

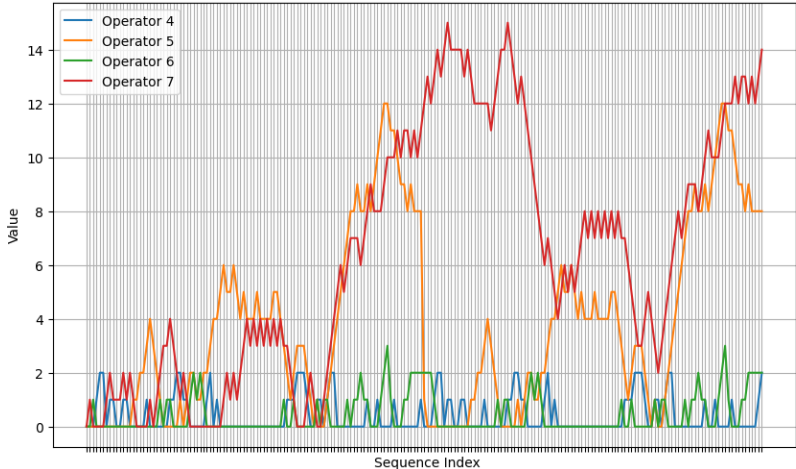


Figure 13: Token-copy task, *initialization*. The top-1 mode of the relative-position histogram is diffuse and nearly uniform prior to training, indicating that the model has no initial bias about which past position to copy from.

Graph 9, Latest Cached Real Positions for fixed_output_gates = False, fixed_reset_gates = False, range = range(0, 75), RE/layer num = 0, first_half = True

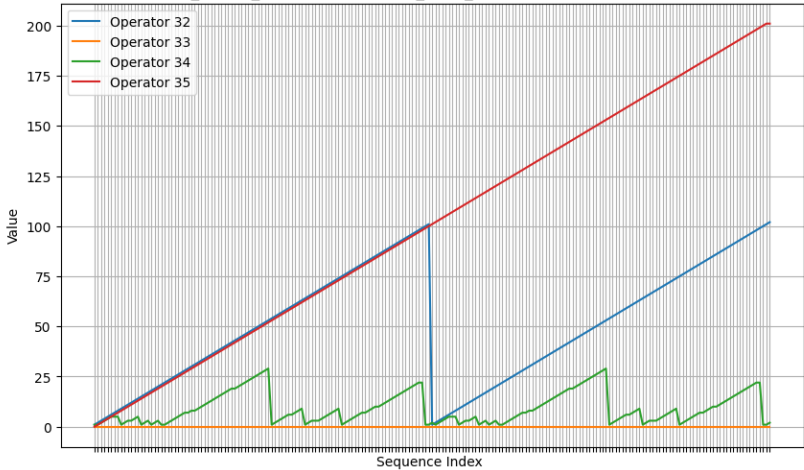


Figure 14: Token-copy task, *after training*. The histogram sharpens dramatically, with the blue query cursor’s mode exactly matching the true offset between each query and its corresponding key—demonstrating precise learned localization. Note that both query and key histograms are learned from scratch from random initialization, demonstrating an emergent coupling of the keys to *uniquely align* with the queries.

Graph 8, Latest Cached Real Positions, range = range(0, 75), RE/layer num = 1, Query Relative Positions, module_num = 1

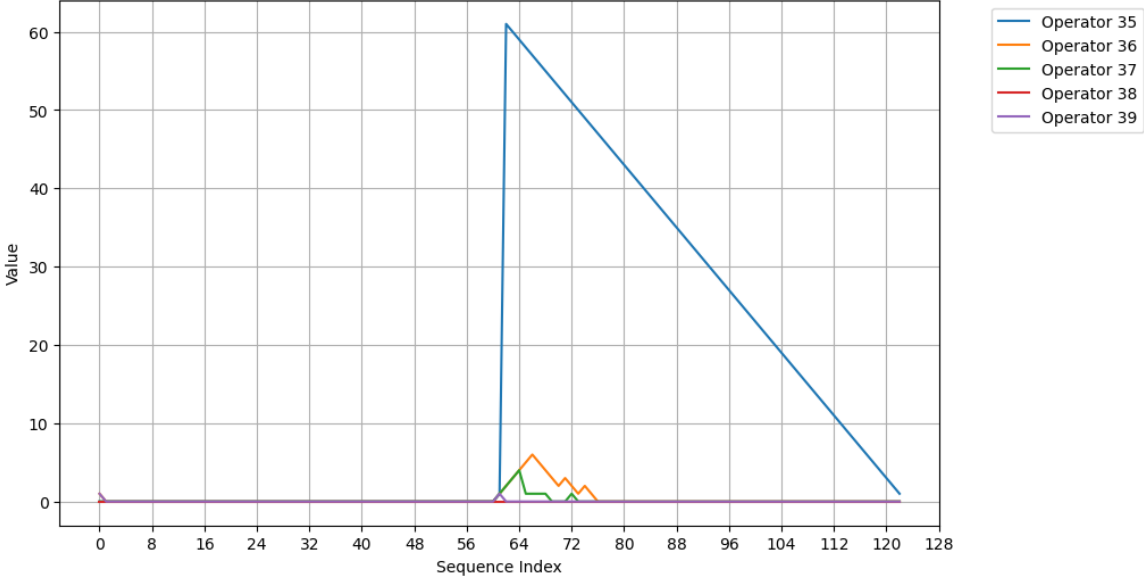


Figure 15: Reverse task. PRISM’s top-1 relative-position mode via the blue cursor tracks the unique start symbol in the source string, enabling correct variable-offset copying even at test lengths far from training.



Figure 16: Addition (chain-of-thought) (3) task at OOD lengths. The full histogram for each query token remains well-structured—peaked around the correct relative positions, attending to earlier digits *via a non-1:1 mapping* to correctly write the chain-of-thought tokens—even when sequence lengths exceed those seen during training.

Graph 6, Latest Cached Real Positions for fixed_output_gates = False, fixed_reset_gates = False, range = range(0, 75), RE/layer num = 0, first_half = True

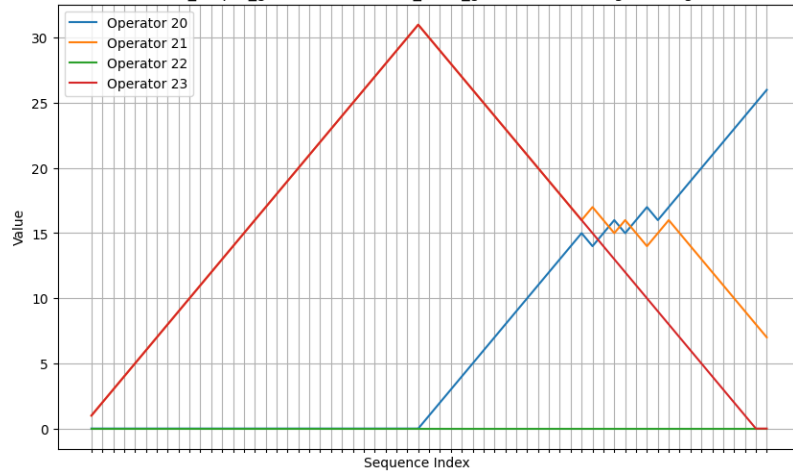
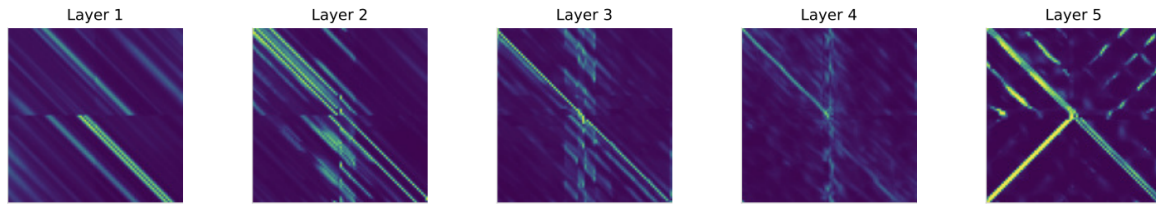
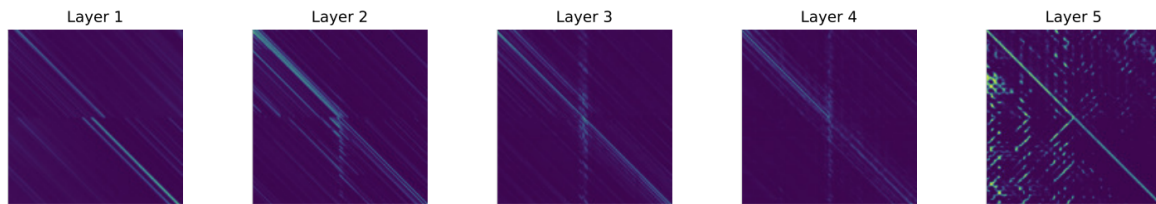


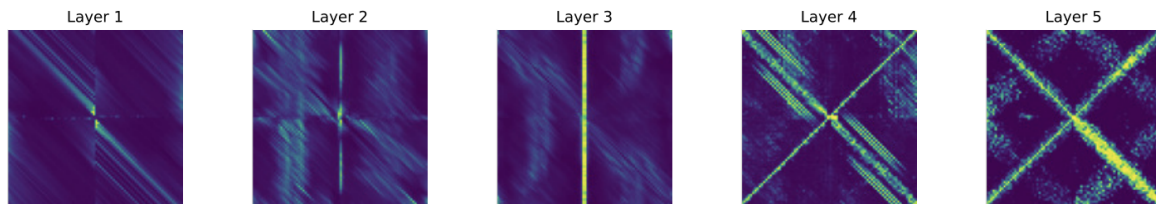
Figure 17: Reverse-string task. The top-1 mode of the positional histogram reveals symmetric displacement patterns that exactly align with the positions required to reconstruct the reversed output, agnostic to input length. The query cursor histogram for operator (cursor) 23 demonstrates an *emergent property* of the model, as both the query and key relative positions had to be learned in order to iterate through the input sequence in reverse.



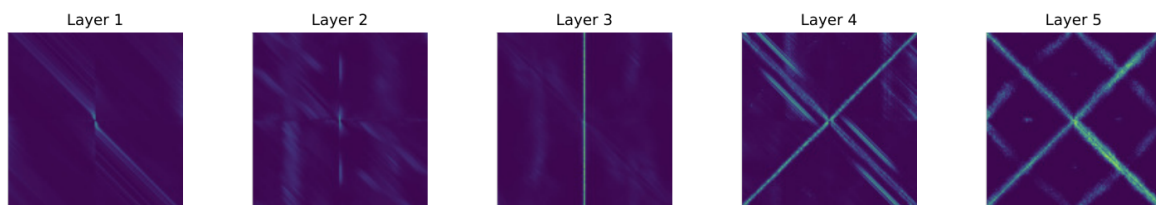
(a) Relative (baseline) with a sequence of length 40 (in-distribution).



(b) Relative (baseline) with a sequence of length 150 (out-of-distribution).



(c) Randomized relative (our method) with a sequence of length 40 (in-distribution).



(d) Randomized relative (our method) with sequence of length 150 (out-of-distribution).

Figure 6: Analysis of the attention matrices for the relative and randomized relative positional encodings on the REVERSE STRING task using sequences of length 40 (i.e., maximum training length) and 150 (i.e., beyond training lengths). We visualize the maximum over the 8 heads per layer (following Csordás et al., 2022) and observe a clear X pattern, which corresponds to the reversal of the sequence. Our randomized relative encodings maintain that pattern on longer sequences, while it breaks down for the standard relative encoding.

Figure 18: Baseline comparison adapted from randomized PEs [Ruoss et al. 2023] on the reverse task. Unlike PRISM’s learned histograms, randomized encodings fail to produce a coherent mode, demonstrating the advantage of data-driven positional distributions.

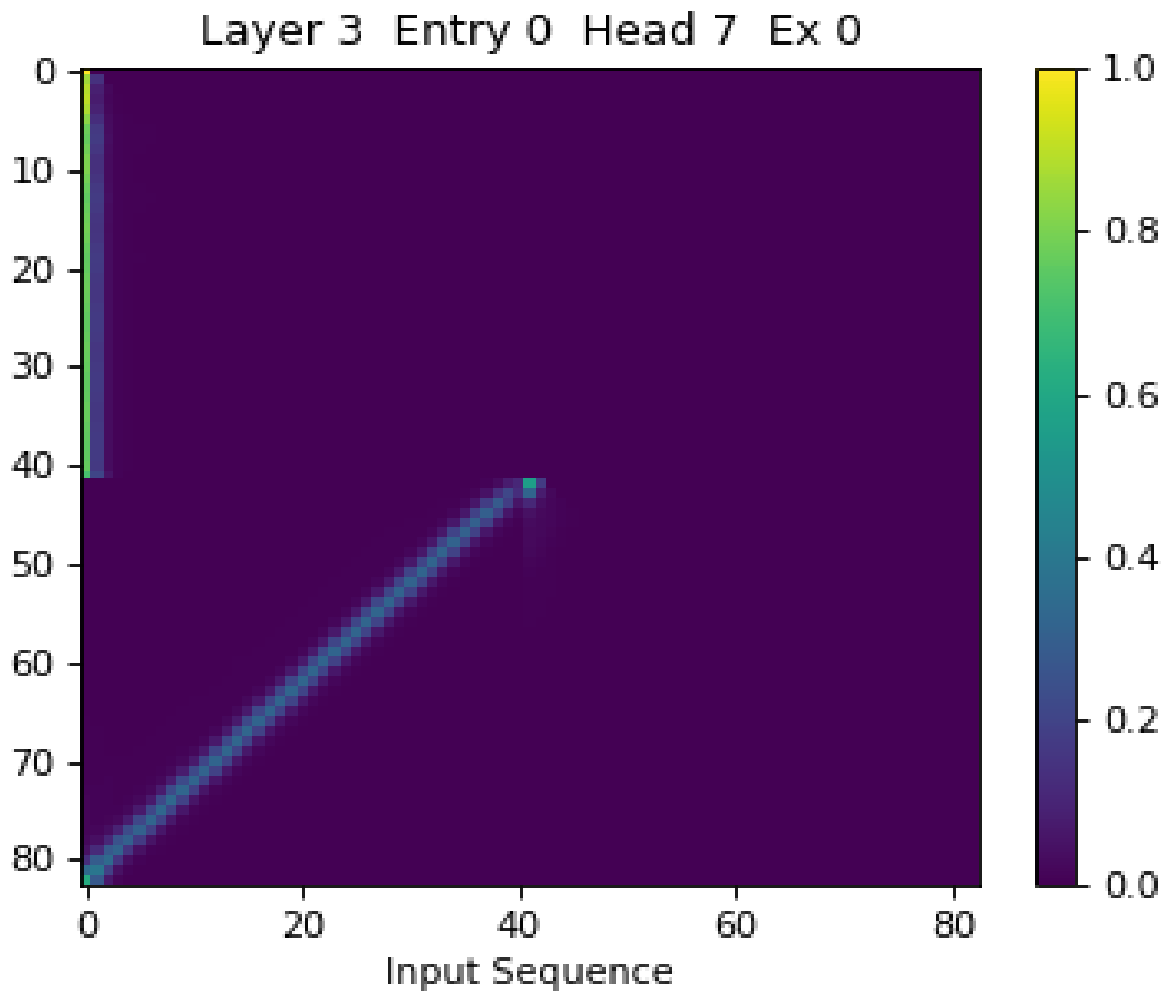


Figure 19: Learned self-attention probabilities on the reverse task (in-distribution) for output sequence length 40 (the maximum trainable length, following Ruoss et al., 2023. PRISM attends selectively to both local neighbors and distant tokens, capturing the two-sided dependencies needed for exact reversal.

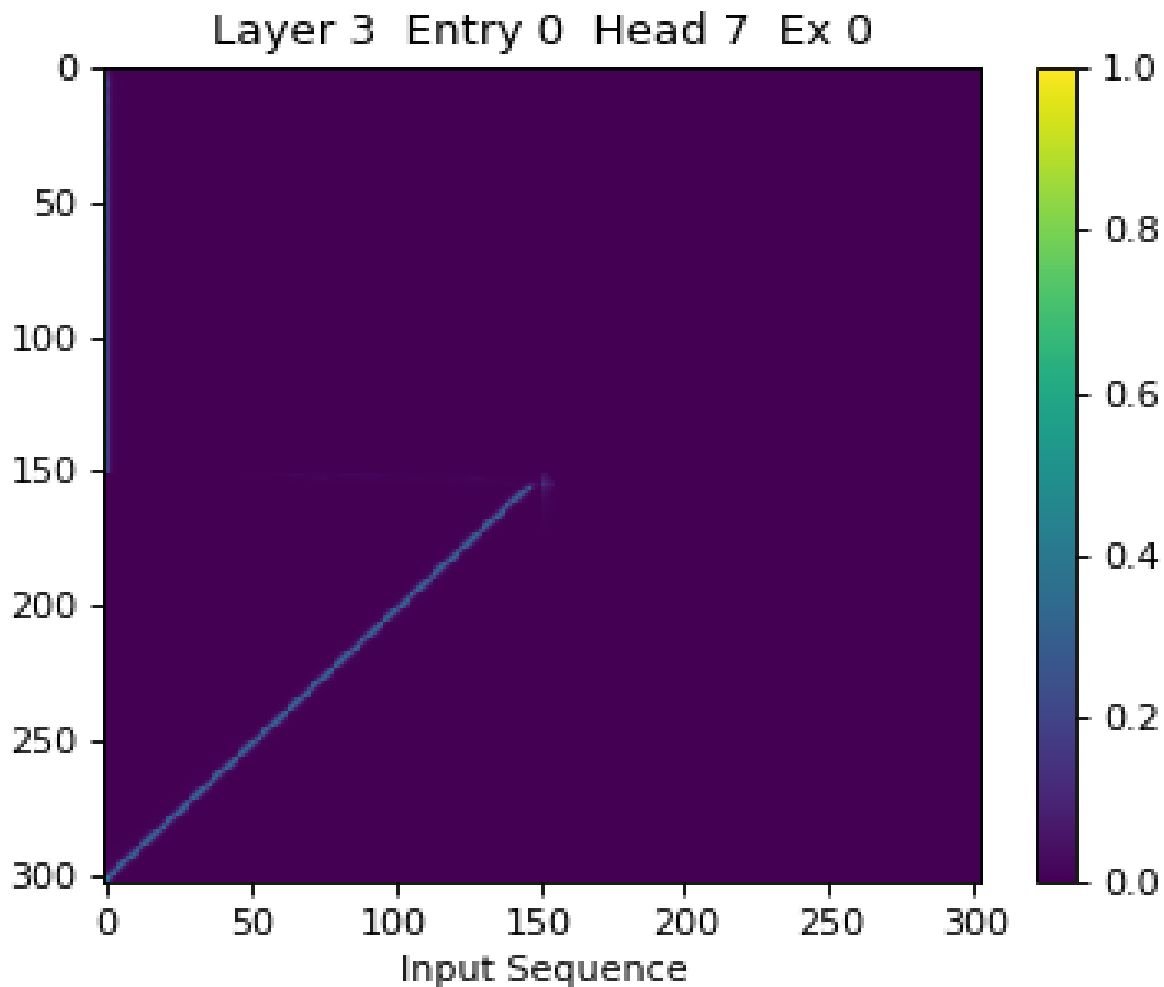


Figure 20: Self-attention probabilities on the reverse task at an OOD length of 150. Unlike Ruoss et al., 2023, the same *sparse* [9] attention pathways persist for much longer sequences, evidencing the model’s ability to generalize its positional reasoning far beyond the training horizon.

C Algorithmic Details

Algorithm 1 Histogram Update per Cursor c with Optional Copy Branch (Symmetric Offsets)

Require: For each cursor $c \in \{1, \dots, C\}$: current histogram $\mathbf{h}_t^{(c)} \in \Delta^{L-1}$ (rows = indices $0 \dots L-1$)

Require: Symmetric support: $L = 2P + 1$, center index $\text{mid} = P$, where index i corresponds to offset $d = i - \text{mid} \in \{-P, \dots, +P\}$

Require: Gate scalars $p_{\text{reset}}^{(c)}, p_{\text{incr}}^{(c)}, p_{\text{decr}}^{(c)}, p_{\text{keep}}^{(c)} \in [0, 1]^B$

Require: (Optional) copy distribution $\mathbf{p}_{\text{copy}}^{(c)} \in \Delta^{L+1}$ (last entry = “no-copy”)

Ensure: Next histogram $\mathbf{h}_{t+1}^{(c)}$

(1) **Aggregate mass**

$$\text{total}^{(c)} = \sum_{i=0}^{L-1} h_t^{(c)}[i] \in \mathbb{R}^B$$

1: Initialize $\mathbf{h}_{t+1}^{(c)} \leftarrow \mathbf{0} \in \mathbb{R}^{L \times B}$

(2) **Reset branch (re-center at offset 0, then take one step)**

$$\begin{aligned} h_{t+1}^{(c)}[\text{mid} + 1] &+= \text{total}^{(c)} p_{\text{reset}}^{(c)} p_{\text{incr}}^{(c)} \quad (\text{clamp at } L-1), \\ h_{t+1}^{(c)}[\text{mid}] &+= \text{total}^{(c)} p_{\text{reset}}^{(c)} p_{\text{keep}}^{(c)}, \\ h_{t+1}^{(c)}[\text{mid} - 1] &+= \text{total}^{(c)} p_{\text{reset}}^{(c)} p_{\text{decr}}^{(c)} \quad (\text{clamp at } 0). \end{aligned}$$

(3) **No-reset branch (shift / keep on symmetric offsets)**

$$\begin{aligned} w_{\text{inc}}^{(c)} &= (1 - p_{\text{reset}}^{(c)}) p_{\text{incr}}^{(c)}, \\ w_{\text{dec}}^{(c)} &= (1 - p_{\text{reset}}^{(c)}) p_{\text{decr}}^{(c)}, \\ w_{\text{keep}}^{(c)} &= (1 - p_{\text{reset}}^{(c)}) p_{\text{keep}}^{(c)}, \\ h_{t+1}^{(c)}[i] &+= h_t^{(c)}[i] w_{\text{keep}}^{(c)}, \\ h_{t+1}^{(c)}[i + 1] &+= h_t^{(c)}[i] w_{\text{inc}}^{(c)} \quad (\text{clamp at } L-1), \\ h_{t+1}^{(c)}[i - 1] &+= h_t^{(c)}[i] w_{\text{dec}}^{(c)} \quad (\text{clamp at } 0). \end{aligned}$$

2: **if** $\mathbf{p}_{\text{copy}}^{(c)}$ **provided then**

(4) **Copy branch**

3: Split $\mathbf{p}_{\text{copy}}^{(c)} = (\mathbf{p}_{\text{pos}}^{(c)}, p_{\text{no-copy}}^{(c)})$, where $\mathbf{p}_{\text{pos}}^{(c)} \in \mathbb{R}^{L \times B}$

4: Scale normal flows: $\mathbf{h}_{t+1}^{(c)} \times = p_{\text{no-copy}}^{(c)}$

5: Add copied mass (per offset-bin $k = 0, \dots, L-1$):

$$h_{t+1}^{(c)}[k] += \mathbf{p}_{\text{pos}}^{(c)}[k].$$

6: **end if**

(5) **Sharpen & renormalize**

$$\mathbf{h}_{t+1}^{(c)} \leftarrow \frac{(\mathbf{h}_{t+1}^{(c)} + \varepsilon)^{\gamma_c}}{\sum_{i=0}^{L-1} (h_{t+1}^{(c)}[i] + \varepsilon)^{\gamma_c}}, \quad \gamma_c > 1$$

7: **return** $\mathbf{h}_{t+1}^{(c)}$

Algorithm 2 Efficient Superposition Embedding per Cursor:

`_get_PE_encoding_vectors_from_scalar_positions_and_norm`

Require: Prob. tensors for queries $\mathbf{P}^{(q)}$ and keys $\mathbf{P}^{(k)}$ each of shape $\mathbb{R}^{C \times B \times S \times r}$, where $C = H \times O$ (number of cursors), $r = \#$ branches.

1:

Require: Sinusoidal table $\mathbf{E} \in \mathbb{R}^{r \times d}$.

2:

Ensure: Embedded streams $\mathbf{E}_q, \mathbf{E}_k \in \mathbb{R}^{B \times H \times O \times S \times d}$.

3: **for in parallel** $X \in \{\mathbf{P}^{(q)}, \mathbf{P}^{(k)}\}$ **do**

4: \triangleright Flatten out cursors, batch, sequence into one “row” dim

$$X_{\text{flat}} \leftarrow \text{reshape}(X, [C \ B \ S, r]) \in \mathbb{R}^{(CBS) \times r}$$

5: \triangleright One SIMD-style mat-mul over branches¹²

$$Z_{\text{flat}} \leftarrow X_{\text{flat}} \times \mathbf{E} \in \mathbb{R}^{(CBS) \times d}$$

6: \triangleright Restore to $[C, B, S, d]$

$$Z \leftarrow \text{reshape}(Z_{\text{flat}}, [C, B, S, d])$$

7: \triangleright Turn $C = H \times O$ back into head \times cursor dims, then permute

$$Z \leftarrow \text{reshape}(Z, [H, O, B, S, d]) \xrightarrow{\text{permute}(2,1,0,3,4)} \underbrace{\in \mathbb{R}^{B \times H \times O \times S \times d}}_{\mathbf{E}_{(\cdot)}}$$

8: \triangleright Exactly as in code’s `_apply_abs_concat_and_ln_optim`:

$$(\mathbf{E}_q, \mathbf{E}_k) \leftarrow \text{_apply_abs_concat_and_ln_optim}(Z, Z, B, H, O, S, d, \text{abs_enc}, \text{ablate_abs_pos_enc})$$

9: **if** $X = \mathbf{P}^{(q)}$ **then**

10: $\mathbf{E}_q \leftarrow Z$

11: **else**

12: $\mathbf{E}_k \leftarrow Z$

13: **end if**

14: **end for**

15: **return** $\mathbf{E}_q, \mathbf{E}_k$

C.1 Absolute-PE Concatenation & Layer-Norm Optimization

This routine is called at the end of the superposition embedding to (1) optionally concatenate an absolute positional embedding branch, and (2) apply either a custom scaling or a projection-free layer-norm:

¹²Instead of materializing r separate d_{model} -dimensional vectors for every branch and every token, we multiply once by the $r \times d_{\text{model}}$ sinusoidal table (a single `einsum`/GEMM). The math is identical but the memory traffic is $O(1/r)$ smaller, and the whole update stays in one SIMD-friendly kernel.

Algorithm 3 `_apply_abs_concat_and_ln_optim`

Require: Encodings $enc_q, enc_k \in \mathbb{R}^{B \times H \times C \times S \times d}$,
1: absolute-PE table $abs_enc \in \mathbb{R}^{\geq S \times d}$, flags `CONCAT_ABS_POSITION_ENCODINGS`,
`MHA_USE_CUSTOM_LN`, `ablate_flag` \equiv `False`

Ensure: Updated enc_q, enc_k of same final shape.

- 2: $C_{\text{base}} \leftarrow C$
- 3: **if** `CONCAT_ABS_POSITION_ENCODINGS` **then** \triangleright concatenate one extra absolute-PE branch
- 4: $C \leftarrow C_{\text{base}} + 1$
- 5: $abs_pe \leftarrow abs_enc[: S][1, 1, 1, S, d] \rightarrow \text{expand}(B, H, 1, S, d)$
- 6: **if** `ablate_flag` **then**
- 7: $abs_pe \leftarrow \mathbf{0}_{B \times H \times 1 \times S \times d}$
- 8: **end if**
- 9: $enc_q \leftarrow \text{cat}(enc_q, abs_pe; \text{dim} = 2)$
- 10: $enc_k \leftarrow \text{cat}(enc_k, abs_pe; \text{dim} = 2)$
- 11: **end if**
- 12: **if** `MHA_USE_CUSTOM_LN` **then** \triangleright global rescaling so norm = \sqrt{d}
- 13: $\alpha \leftarrow \text{sinusoidal_encoding_vector_norm_vs_d_model}(d)$
- 14: $scale \leftarrow \frac{\sqrt{d}}{\sqrt{C \cdot \alpha^2}}$
- 15: $enc_q \cdot = scale, enc_k \cdot = scale$
- 16: **else** \triangleright mean-free LayerNorm across $[C, S]$ per head
- 17: **assert** enc_q, enc_k shaped (B, H, C, S, d)
- 18: $enc_q \rightarrow \text{permute}(0, 1, 3, 2, 4) [B, H, S, C, d]$
- 19: $enc_k \rightarrow \text{permute}(0, 1, 3, 2, 4) [B, H, S, C, d]$
- 20: $enc_q \leftarrow enc_q / \|enc_q\|_{(-2, -1)} \times \sqrt{d}$
- 21: $enc_k \leftarrow enc_k / \|enc_k\|_{(-2, -1)} \times \sqrt{d}$
- 22: $enc_q \rightarrow \text{permute}(0, 1, 3, 2, 4), enc_k \rightarrow \text{permute}(0, 1, 3, 2, 4)$
- 23: **end if**
- 24: **return** enc_q, enc_k

Algorithm 4 Position-Aware Attention Scores (`_findPositionScores`)

Require: Encodings $enc_q, enc_k \in \mathbb{R}^{B \times H \times C \times S \times d}$ $\triangleright C$ =cursors per head**Require:** Learned scaling factors $\alpha \in \mathbb{R}^{H \times C}$ (in code: $\alpha \equiv \text{POST_QK_SCALING_FACTORS_MULTIPLIER}$),1: `NEGATIVE_COEFFS_ALLOWED = false`**Ensure:** $scores, position_scores \in \mathbb{R}^{B \times H \times S \times S}$ 2: $(B, H, C, S, d) \leftarrow \text{shape}(enc_q)$ \triangleright cursor index $c = 1, \dots, C$ 3: **for all** $b = 1, \dots, B; h = 1, \dots, H; c = 1, \dots, C; i, j = 1, \dots, S$ **do**

$$scores_3[b, h, c, i, j] \leftarrow \langle enc_q[b, h, c, i, :], enc_k[b, h, c, j, :] \rangle$$

4: **end for** \triangleright **Post-scaling (always nonnegative):**5: $\beta[h, c] \leftarrow |\alpha[h, c]|$ 6: $scores_3[b, h, c, i, j] \cdot = \beta[h, c]$ \triangleright **Sum out cursors:**

$$scores_2[b, h, i, j] = \sum_{c=1}^C scores_3[b, h, c, i, j]$$

7: $N \leftarrow C \times d$ \triangleright **Final normalization:**

$$scores_{final}[b, h, i, j] = \frac{scores_2[b, h, i, j]}{\sqrt{N}}$$

8: $position_scores \leftarrow scores_{final}$ 9: **return** $scores, position_scores$

D SCAN-CoT Length Distributions

Here we show histograms of token-length distributions for the SCAN dataset.

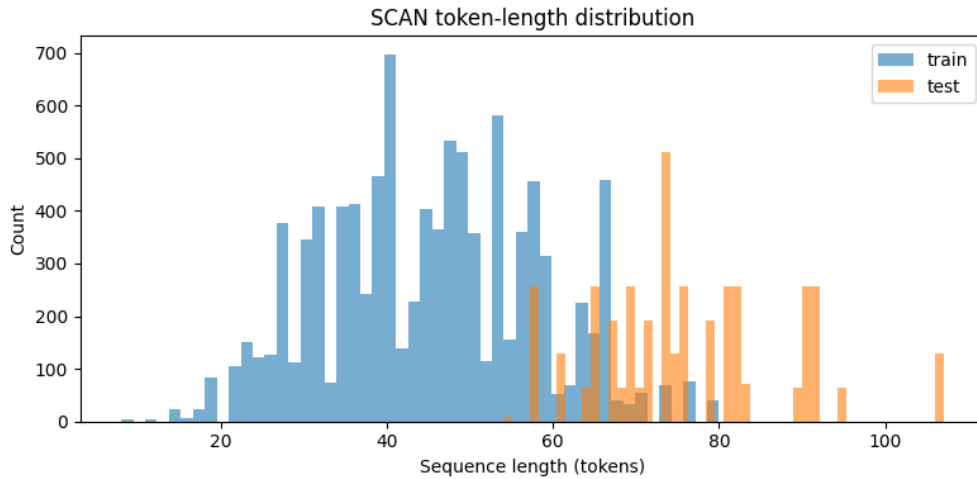


Figure 21: Full-sequence lengths, SCAN train and test split.

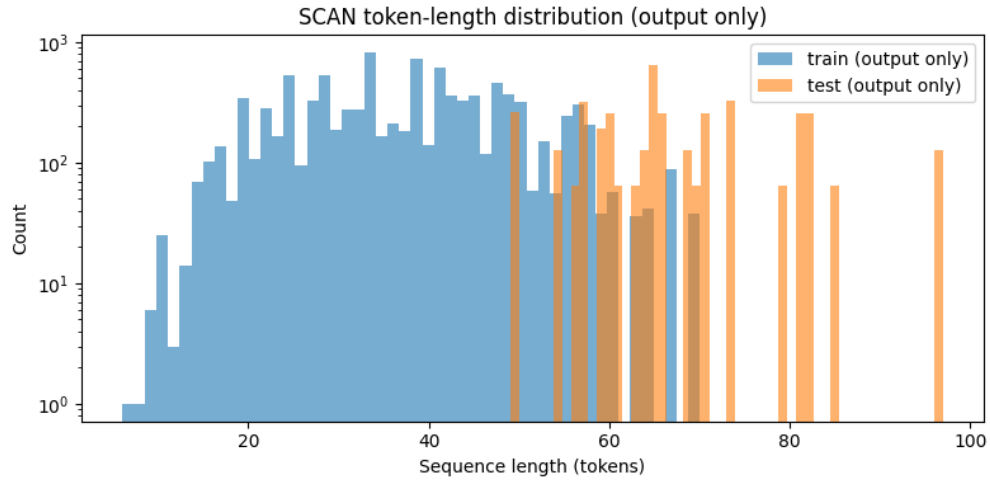


Figure 22: Output-only lengths (tokens right of “=”) on a log scale.

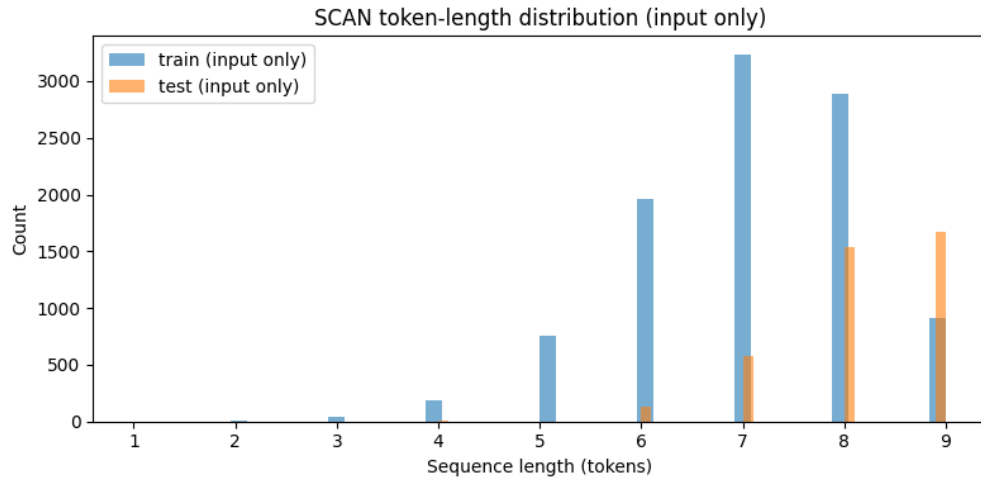


Figure 23: Input-only lengths (tokens left of “=”).

References

- [1] Amir Mansourian Ali Veisi. *Context-aware Biases for Length Extrapolation*. arXiv preprint arXiv:2501.12345. 2025.
- [2] Hanseul Cho et al. “Position Coupling: Improving Length Generalization of Arithmetic Transformers Using Task Structure”. In: *Advances in Neural Information Processing Systems*. Vol. 37. 2024. URL: https://proceedings.neurips.cc/paper_files/paper/2024/file/27aa3a0e6d63db269977bb2Paper-Conference.pdf.
- [3] Grégoire Delétang et al. “Neural Networks and the Chomsky Hierarchy”. In: *International Conference on Learning Representations*. 2023. URL: <https://openreview.net/forum?id=WbxHAzkeQcn>.
- [4] Shaoxiong Duan, Yining Shi, and Wei Xu. *From Interpolation to Extrapolation: Complete Length Generalization for Arithmetic Transformers*. arXiv preprint arXiv:2310.11984. 2023.
- [5] Nouha Dziri et al. “Faith and Fate: Limits of Transformers on Compositionality”. In: *arXiv preprint arXiv:2305.18654* (2023). NeurIPS 2023 Spotlight. URL: <https://arxiv.org/abs/2305.18654>.
- [6] Nelson Elhage et al. *A Mathematical Framework for Transformer Circuits*. Transformer Circuits Thread. Dec. 2021. URL: <https://transformer-circuits.pub/2021/framework/index.html>.
- [7] Nelson Elhage et al. “Toy Models of Superposition”. In: *arXiv preprint arXiv:2209.10652* (2022). URL: <https://arxiv.org/abs/2209.10652>.
- [8] Ying Fan et al. “Looped Transformers for Length Generalization”. In: *International Conference on Learning Representations*. 2025.
- [9] Noah Golowich et al. *The Role of Sparsity for Length Generalization in Transformers*. arXiv preprint arXiv:2502.16792. 2025. URL: <https://arxiv.org/pdf/2502.16792>.
- [10] Pengcheng He et al. “DeBERTa: Decoding-enhanced BERT with Disentangled Attention”. In: *International Conference on Learning Representations*. 2021. URL: <https://openreview.net/forum?id=XPZiaotutsD>.
- [11] Zhenyu He et al. “Two Stones Hit One Bird: Bilevel Positional Encoding for Better Length Extrapolation”. In: *International Conference on Machine Learning*. 2024.
- [12] Kaiying Hou et al. *Universal Length Generalization with Turing Programs*. arXiv preprint arXiv:2407.03310. 2024.
- [13] Amirhossein Kazemnejad et al. “The Impact of Positional Encoding on Length Generalization in Transformers”. In: *Advances in Neural Information Processing Systems*. Vol. 36. 2023.
- [14] Brenden M. Lake and Marco Baroni. “Generalization without systematicity: On the compositional skills of sequence-to-sequence recurrent networks”. In: *International Conference on Machine Learning*. 2018.
- [15] Nayoung Lee et al. *Self-Improving Transformers Overcome Easy-to-Hard and Length Generalization Challenges*. arXiv preprint arXiv:2502.01612. 2025. URL: <https://arxiv.org/pdf/2502.01612>.
- [16] Xiaoran Liu et al. *Thus Spake Long-Context Large Language Model*. arXiv preprint arXiv:2502.17129. 2025.

- [17] Sean McLeish et al. “Transformers Can Do Arithmetic with the Right Embeddings”. In: *Advances in Neural Information Processing Systems*. 2024.
- [18] Ben Mildenhall et al. “Neural Radiance Fields (NeRF): Representing Scenes as Neural Radiance Fields for View Synthesis”. In: *European Conference on Computer Vision*. 2020. URL: <https://www.matthewtancik.com/nerf>.
- [19] Catherine Olsson et al. “In-context Learning and Induction Heads”. In: *arXiv preprint arXiv:2209.11895* (2022). URL: <https://arxiv.org/abs/2209.11895>.
- [20] Anthropic PBC. *Privileged Bases in the Transformer Residual Stream*. Anthropic blog post. Mar. 2023. URL: <https://www.anthropic.com/research/privileged-bases-in-the-transformer-residual-stream>.
- [21] Anthropic PBC. *Superposition, Memorization, and Double Descent*. Anthropic blog post. Jan. 2023. URL: <https://www.anthropic.com/research/superposition-memorization-and-double-descent>.
- [22] Anian Ruoss et al. “Randomized Positional Encodings Boost Length Generalization of Transformers”. In: *Proceedings of the 61st Annual Meeting of the Association for Computational Linguistics*. 2023.
- [23] David Saxton et al. “Analysing Mathematical Reasoning Abilities of Neural Models”. In: *International Conference on Learning Representations*. 2019.
- [24] Richard S. Sutton. *The Bitter Lesson*. Blog post, Incomplete Ideas. 2019. URL: <https://www.incompleteideas.net/IncIdeas/BitterLesson.html>.
- [25] Matthew Tancik et al. “Fourier Features Let Networks Learn High Frequency Functions in Low Dimensional Domains”. In: *Advances in Neural Information Processing Systems*. Vol. 33. 2020. URL: <https://arxiv.org/abs/2006.10739>.
- [26] Ashish Vaswani et al. “Attention is All You Need”. In: *Advances in Neural Information Processing Systems*. 2017.
- [27] Gail Weiss, Yoav Goldberg, and Eran Yahav. “Inferring Algorithmic Patterns with Stack-Augmented Recurrent Nets”. In: *Conference of the North American Chapter of the Association for Computational Linguistics*. 2018.
- [28] Gail Weiss, Yoav Goldberg, and Eran Yahav. “Thinking Like Transformers”. In: *International Conference on Machine Learning*. 2021.
- [29] Liang Zhao et al. “Length Extrapolation of Transformers: A Survey from the Perspective of Positional Encoding”. In: *Findings of the Association for Computational Linguistics: EMNLP 2024*. Association for Computational Linguistics, Nov. 2024. DOI: [10.18653/v1/2024.findings-emnlp.582](https://doi.org/10.18653/v1/2024.findings-emnlp.582). URL: <https://aclanthology.org/2024.findings-emnlp.582/>.
- [30] Chuanyang Zheng et al. “DAPE: Data-Adaptive Positional Encoding for Length Extrapolation”. In: *Advances in Neural Information Processing Systems*. 2024.
- [31] Hattie Zhou et al. “What Algorithms can Transformers Learn? A Study in Length Generalization”. In: *International Conference on Learning Representations*. 2024.